

University of Washington
Department of Civil and Environmental Engineering



AN EVALUATION OF THE EFFECTS OF
ANTHROPOGENIC ACTIVITY ON
STREAMFLOW IN THE COLUMBIA RIVER
BASIN

Robin Kirschbaum
Dennis P. Lettenmaier



Water Resources Series
Technical Report No.156
September 1997

Seattle, Washington
98195

Department of Civil Engineering
University of Washington
Seattle, Washington 98195

**AN EVALUATION OF THE EFFECTS OF ANTHROPOGENIC
ACTIVITY ON STREAMFLOW IN THE COLUMBIA RIVER BASIN**

Robin Kirschbaum
Dennis P. Lettenmaier

Water Resources Series
Technical Report No. 156

September 1997

ABSTRACT

The effects of changes in vegetation in the last century on Columbia basin streamflow were assessed using a macroscale hydrological model, which parameterizes the effects of vegetation on evapotranspiration and hence streamflow. The spatial distribution of vegetation species and age were represented using remote sensing-based maps of current vegetation, and reconstructed maps of historical vegetation. The historical vegetation information represented a best estimate of conditions in the early 1900's, for which vegetation maps were prepared by the interagency Interior Columbia Basin Ecosystem Management Project. Hydrologic simulations were performed for the sixteen year period 1980-95, using the two vegetation scenarios.

The hydrologic model was calibrated to the Columbia River basin at one quarter-degree latitude-longitude resolution using current scenario vegetation information, and soil parameters determined from literature, data, and manual calibration. Relative differences in predicted streamflow were evaluated graphically and statistically on monthly, seasonal and annual time scales. The largest positive differences (current condition exceeding historical) in mean streamflow were predicted in the Corra Linn, Revelstoke, and Mica subbasins in the northern portion of the basin, all of which exceeded six percent on an annual basis. The annual changes were traceable mostly to decreased summer evaporation due to less mature current vegetation, the effect of which was to increase mean summer streamflow by 8.5 percent (Mica) to 10.8 percent (Cora Linn). The largest negative difference was for the Waneta subbasin (Pend O'Reille river), which had a mean annual flow decrease of about nine percent, apparently due to inferred increase in vegetation maturity due to fire suppression. Mean annual flow changes for all other subbasins were less than two percent. Although extensive changes in vegetation occurred in some regions where streamflow changes were projected to be minimal, in many cases the associated differences in model parameters were small. The predicted change in mean annual streamflow at the basin outlet was approximately zero. Model-predicted changes in streamflow were found to be highly sensitive to the specified distribution of roots between model layers. Changes in the model's parameterization of root extraction of moisture from the model soil layers, and inclusion of a scheme that represents directly the effects of vegetation on snow accumulation and ablation, could change the predictions of streamflow sensitivity to vegetation changes.

Table of Contents

1. INTRODUCTION	1
1.1 STUDY OBJECTIVES	2
1.2 APPROACH	2
2. BACKGROUND INFORMATION.....	6
2.1 PHYSICAL DESCRIPTION OF THE STUDY AREA	6
2.2 OVERVIEW OF HUMAN SETTLEMENT IN THE COLUMBIA RIVER BASIN.....	11
2.3 LAND USE AND LAND COVER CHANGES.....	12
2.3.1 Forests	12
2.3.1.1 Timber harvest.....	13
2.3.1.2 Dry forest	14
2.3.1.3 Moist forest	15
2.3.1.4 Cold forests	16
2.3.2 Rangeland	16
2.3.2.1 Livestock grazing.....	17
2.3.2.2 Fire regimes	18
2.3.2.3 Introduction of exotic plants	19
2.3.3 Urbanization	21
2.3.4 Agriculture.....	22
3. MODEL COMPONENTS	24

3.1 SNOW ABLATION/ACCUMULATION MODEL	26
3.2 VIC-2L LAND SURFACE MODEL.....	27
3.3 ROUTING MODEL.....	31
4. MODEL IMPLEMENTATION	36
4.1 INPUT DATA.....	36
4.1.1 Digital elevation model.....	36
4.1.2 Meteorological data	37
4.2 PARAMETER ESTIMATION	42
4.2.1 Snow Model Parameters	42
4.2.2 Soil parameters	46
4.2.3 Vegetation parameters	56
4.2.3.1 Current and historical cover class maps	60
4.2.3.2 Parameter assignment.....	75
4.3 CALIBRATION AND TEST RESULTS	82
4.4 MEAN ANNUAL PRECIPITATION, RUNOFF AND EVAPORATION	82
4.5 RELATIVE BIAS	85
4.6 RELATIVE ROOT MEAN SQUARE ERROR.....	85
4.7 MONTHLY HYDROGRAPHS.....	86
5. CURRENT AND HISTORICAL SCENARIO SIMULATION RESULTS.....	94
5.1 RELATIVE PERCENT DIFFERENCE	94
5.2 MEAN MONTHLY HYDROGRAPHS AND RELATIVE PERCENT DIFFERENCE	96

5.2.1.1 Sensitivity analysis of the root distribution parameter	106
6. CONCLUSIONS	119
7. REFERENCES	122

List of figures

Figure 2.1 Map of the Columbia River basin.....	7
Figure 2.2 30-arcsecond Digital Elevation Model of the Columbia basin.....	9
Figure 2.3 Location of forested, rangeland, agricultural and urban areas within the Columbia River basin.	23
Figure 3.1 Schematic modeling approach.....	25
Figure 3.2 Flow direction network input to the routing model.	33
Figure 4.1 Location of precipitation and temperature data stations.	39
Figure 4.2 Simulated snow areal extent.	43
Figure 4.3 Snow areal extent observed by GOES satellite.....	44
Figure 4.4 STATSGO derived soil parameters.....	51
Figure 4.5 Subbasins contributing to nine naturalized flow locations.....	53
Figure 4.6 Current vegetation map (CVM).....	58
Figure 4.7 Historical vegetation map (HVM).....	59
Figure 4.8 Histogram of VIC-2L vegetation cover types verses SiB cover types in the U.S. portion of the CRB.	69
Figure 4.9 Histogram of SiB cover types in Canada (before reclassifying).....	70
Figure 4.10 Histogram of VIC-2L cover types in Canada (after reclassifying).....	71

Figure 4.11 Histograms of NDVI for combinations of coniferous cover types and structural stages.	73
Figure 4.12 Mean annual water balance for the calibration period.	84
Figure 4.13 Simulated and naturalized mean monthly streamflow for calibration period October, 1983 - September, 1986.	90
Figure 4.14 Simulated and naturalized mean monthly streamflow for test period October, 1986 - September, 1989.	91
Figure 5.1 Mean monthly hydrographs for the current and historical vegetation scenarios and relative percent difference.	97
Figure 5.2 Simulated mean monthly a) current, b) historical and c) percent difference in evaporation for the month of August at Revelstoke.	100
Figure 5.3 Simulated mean monthly a) current, b) historical and c) percent difference in baseflow for the month of October at Revelstoke.	101
Figure 5.4 Simulated mean monthly a) current, b) historical and c) percent difference in evaporation for the month of May at Revelstoke.	102
Figure 5.5 VIC-2L results from point sensitivity analysis for the month of August.	110
Figure 5.6 VIC-2L results from point sensitivity analysis for the month of May.	111
Figure 5.7 Sensitivity analysis of vegetation parameter f2 performed for Corra Linn for the test period October, 1986 to September, 1989.	118

List of tables

Table 4.1	Depths of eleven STATSGO soil layers.....	48
Table 4.2	Porosity and saturated hydraulic conductivity as a function of soil type ^a	49
Table 4.3	Subbasin river mile and drainage areas.	54
Table 4.4	Range of calibrated soil parameters. The symbol “*” indicates that the parameter was heavily adjusted.	56
Table 4.5	Description of VIC-2L cover types.	64
Table 4.6	SiB cover types and remap table used for reclassification.	67
Table 4.7	Means and standard deviations for NDVI coupled with various combinations of coniferous forest and structural stage.	74
Table 4.8	Look-up table used to assign parameters to VIC-2L vegetation classes.	80
Table 4.9	Relative bias and root mean square error for the calibration period.....	92
Table 4.10	Relative bias and root mean square error for the test period.	93
Table 5.1	Annual and seasonal RPD for all locations.	95
Table 5.2	Subbasin-wide dominant vegetation classes and parameter values for the current and historical scenarios at Revelstoke and Mica.	98
Table 5.3	Current and historical scenario vegetation parameters at Waneta.....	104
Table 5.4	Soil parameter used values for the point sensitivity analysis of f2.....	108
Table 5.5	Range of calibrated soil parameters for Corra Linn.....	113

ACKNOWLEDGEMENTS

The research described in this report is based on the Masters thesis of the first author. Funding was provided by a Cooperative Agreement between the U.S. Forest Service and the University of Washington. The advice of University of Washington Professors Richard N. Palmer and Derek Booth, who served on the first author's thesis committee, is greatly appreciated.

Thanks also go to the many people who provided data and information used in this study. Peter Thornton (Ph.D. student at University of Montana, Department of Forest Resources) assisted in obtaining the data used to define the current and historical vegetation scenarios and in assessing vegetation parameters. Professor Tom Hinckley of the Department of Forest Resources at University of Washington provided information which was helpful in assessing and analyzing the sensitivity of model predictions to vegetation parameters. Dr. Dag Lohmann at Princeton University, and Mr. Keith Cherkauer at the University of Washington, developed the code for the VIC-2L hydrologic model which was used in this study. Several students in the Department of Civil Engineering at the University of Washington dedicated their time and energy towards the completion of this study. Thanks are especially due to graduate students and staff in the Hydrology group at the UW Civil Engineering Department, including Bart Nijssen, Keith Cherkauer, Laura Bowling, Pascal Storck, Tony Dubin, Jonathon LaMarche and Greg O'Donnell.

1. Introduction

Over the last several decades, the treatment of vegetation in macroscale hydrologic models has evolved from the simple bucket model of Manabe et al. (1965) to highly developed parameterization schemes which predict the partitioning of water and energy at the Earth's surface (Wood, 1991). Recent advances in data acquisition, such as remote sensing, have greatly increased the quality and availability of high resolution vegetation data. Geographic Information Systems (GIS) provide a tool for analyzing spatial information, such as vegetation, digital elevation and soils data layers, and integrating the information into hydrologic models.

The evolution of more sophisticated hydrology - vegetation models provides a mechanism for evaluation of the effects of vegetation change on the atmospheric branch of the hydrologic cycle (e.g., the work of Dickinson et al. (1986) and others, which has evaluated the effects of Amazonian deforestation on climate), as well as the effects of vegetation changes on terrestrial hydrologic fluxes. The latter application is the focus of this thesis.

The motivation for this study derives from the work of the Interior Columbia Basin Ecosystem Management Project (ICBEMP), which recently conducted an integrated assessment of the effects of changes in vegetation in the Columbia River basin on the regional ecosystem (Quigley and Arbelbide, 1996). The purpose of their study was to

develop scientifically sound, ecosystem-based land management alternatives for adoption by the Department of Agriculture and the Department of Interior. An obvious question that was not addressed by ICBEMP was how the vegetation changes they identified have affected the hydrology of the Columbia basin. In this study, the vegetation data that were produced as a part of the ICBEMP study were used to represent “current” and “historical” vegetation scenarios in a macroscale hydrologic model, which was able to perform quantitative predictions of the effects of changes in vegetation on streamflow in the Columbia River basin.

1.1 Study objectives

The primary objective of this study is to evaluate the effects of anthropogenic changes in vegetation on streamflow in the Columbia River basin. A secondary objective is to assess the sensitivity of predicted streamflow changes to selected hydrologic model parameters.

1.2 Approach

The strategy used to evaluate the macroscale hydrologic effect of changes in vegetation related to human activity is comparison of streamflow predictions based on current (1990) and historical (early 1900's) vegetation scenarios. The historical frame of reference is the period of time just prior to significant Euro-American settlement in the

region. Although the basin was actually settled in the mid 1800's, the later target date used in this study is concurrent with the time of earliest consistent archival of information regarding vegetation. Changes in vegetation are represented by the assignment of vegetation parameters extracted from spatial maps of current and historical cover type and structural stage prepared by ICBEMP (Quigley and Arbelbide, 1996). ICBEMP was developed under the U.S. Department of the Interior (USDI) and the Department of Agriculture (USDA) to develop land management alternatives that maintain the integrity of the ecosystems within the region. The U.S. portion of the Interior Columbia Basin consists of 145 million acres of land and extends from the eastern Cascades to the western Rockies.

Using data bases developed by ICBEMP, it is possible to combine maps of cover type and structural stage to create vegetation class maps for current and historical scenarios, which are referred to as Current Vegetation Map (CVM) and Historical Vegetation Map (HVM), respectively. Cover type defines the type of vegetation (i.e., coniferous forest, deciduous forest, shrub, etc.) and structural stage defines the species and/or condition of vegetation during different phases of succession (Quigley and Arbelbide, 1996). A vegetation class represents a unique combination of cover type and structural stage in this application. For both the current and historical scenarios, vegetation parameters needed for hydrological modeling can be assigned according to the grid cell vegetation class. The approach used in this study to prescribe vegetation parameters is described in more detail in Chapter 4.

The hydrologic model used in this study is the Variable Infiltration Capacity - 2 Layer (VIC-2L) model of Liang et al. (1994). It is a hydrologically-based macroscale soil-vegetation-atmosphere transfer scheme (SVATS), which parameterizes the effect of subgrid heterogeneity of soil properties on runoff production. The model has previously been applied to the Columbia River basin at one-degree spatial resolution by Nijssen et al. (1997). In this study, the model was implemented and calibrated to the Columbia River basin at quarter-degree spatial resolution using current scenario vegetation parameters and soil parameters estimated from spatially distributed data bases, by manual search for some parameters and from literature values for others (see Chapter 4 for details on parameter estimation).

Once calibrated, the model was used to simulate streamflow for the current and historical scenarios at nine locations within the basin. The resulting streamflow predictions were compared using the current vegetation scenario as the control condition. The relative differences in streamflow were evaluated on monthly, seasonal and annual time scales at each location. Three general tools were used to analyze model output: i) analysis of mean annual water balance, ii) comparison of seasonal and annual relative bias and relative root mean square error and iii) comparison of current and historical scenario simulated mean monthly hydrographs.

The secondary objective was accomplished by simulating current and historical scenario streamflow using relevant soil and vegetation parameters. Selected model parameters were varied as a function of structural stage in small increments, and the

resulting water partition over a single grid-cell and routed monthly hydrographs were compared.

2. Background Information

In this chapter, the portion of the Columbia River basin which was considered in this study is described. The history of human settlement in the CRB, beginning in the late 1800's and continuing through the late 1900's, and the effects of various land use activities on streams and vegetation within the basin are also discussed.

2.1 Physical description of the study area

The Columbia River basin (CRB) drains roughly 690,000 km² and covers part or all of seven states in the northwestern United States (Washington, Oregon, Idaho, Montana, Wyoming, Nevada and Utah) and part of British Columbia (B.C.) in southwestern Canada. Approximately 85 percent of the basin lies in the U.S. and the remaining 15 percent is in Canada. The Columbia River originates at Columbia Lake on the western slopes of the Canadian Rockies. The Snake River, which is the largest tributary, joins the Columbia downstream of the Tri-Cities in southeastern Washington. The Snake River contributes roughly 30% of the total flow at The Dalles. Figure 2.1 shows the basin and the major tributaries. For this study, only the portion of the basin upstream of The Dalles was modeled. Thus, the westside areas draining the Willamette, Cowlitz and Lewis rivers, which have much different hydroclimatology than the rest of the basin, lie outside of the modeled region.

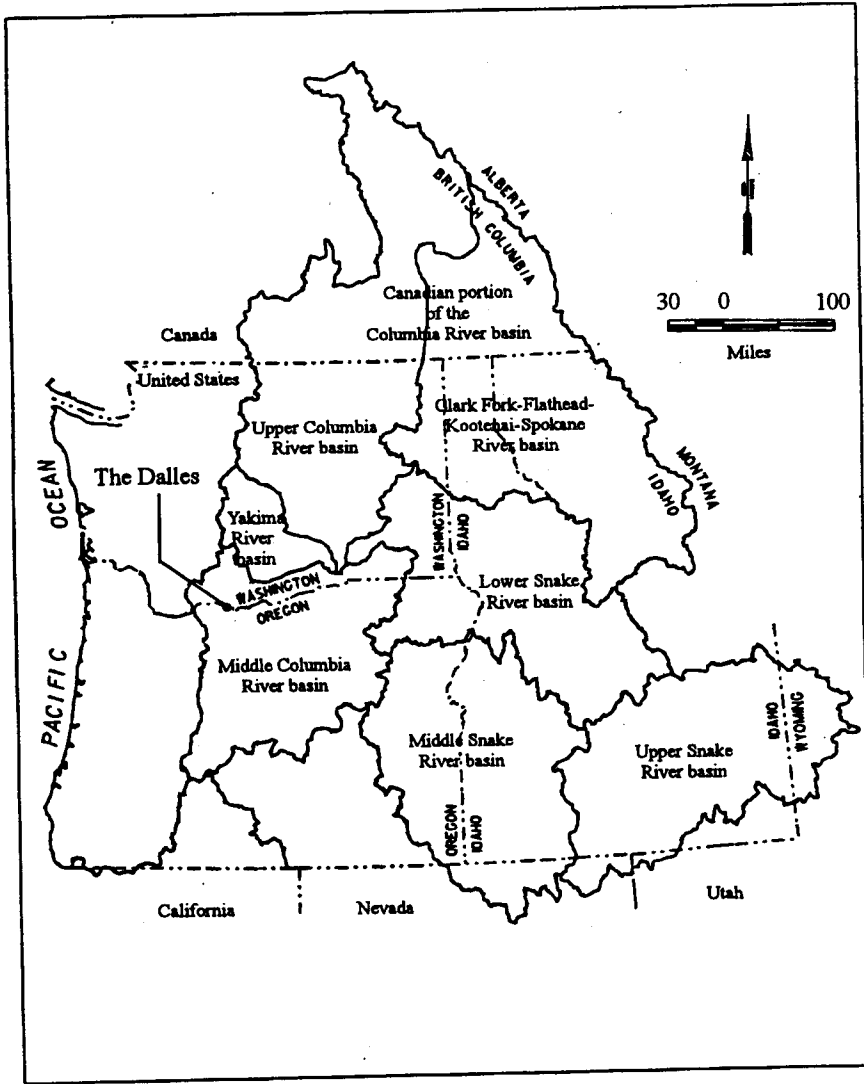


Figure 2.1 Map of the Columbia River basin

The CRB is topographically complex, with the Cascade and Rocky Mountains forming the western and eastern edges, respectively. Above The Dalles, elevation ranges from 150 to 3,000 m. Two major plateaus, the Columbia and Snake Plateaus, occupy much of the central portion of the basin. Figure 2.2 shows the topography of the basin as extracted from a 30-arcsecond USGS Digital Elevation Model (DEM).

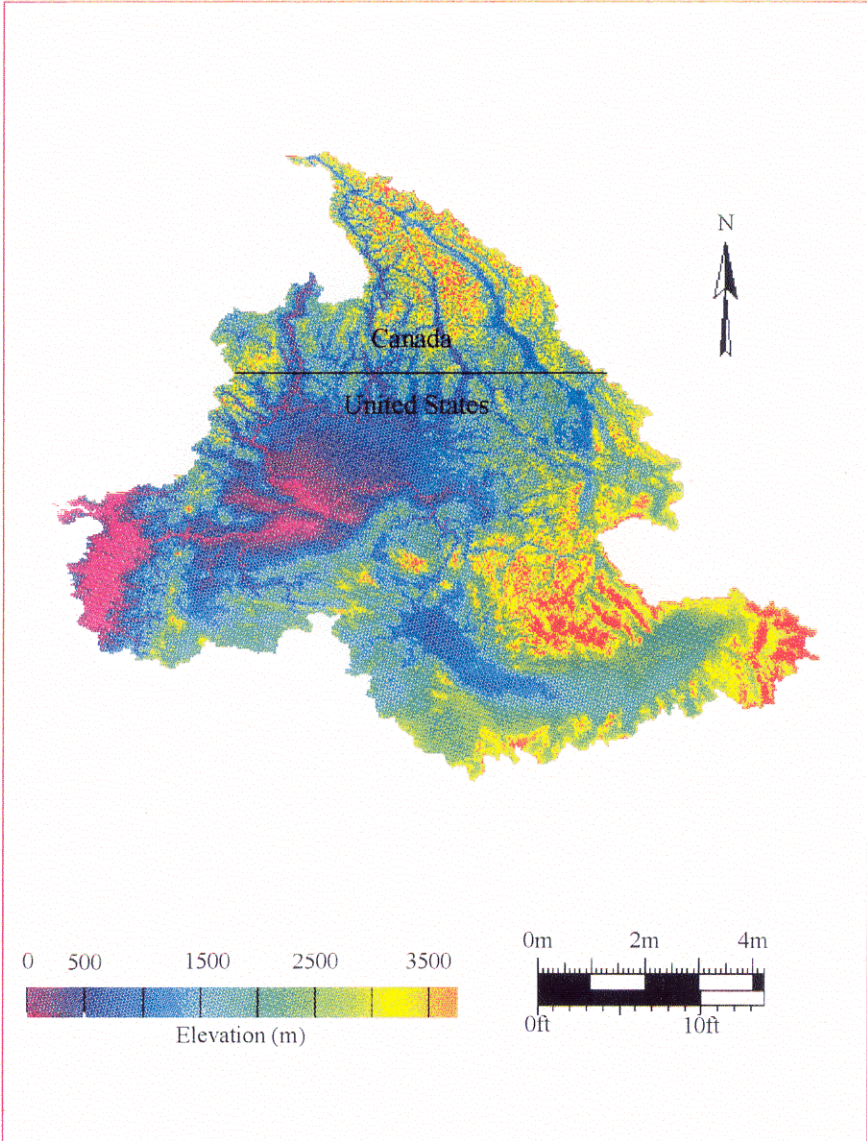


Figure 2.2 30-arcsecond Digital Elevation Model of the Columbia basin.

Topography exerts a strong control on precipitation within the basin. Most of the annual precipitation in the mountainous headwaters (from which most of the streamflow at The Dalles is derived) falls in the winter months as snow which is stored in deep snow packs during the winter. Spring snowmelt dominates the annual hydrograph of most tributaries, with approximately 60 percent of the runoff occurring in May, June and July, on average. Annual precipitation within the modeled region is highest on the western boundary of the basin just above The Dalles, where it ranges from 1850 to 2500 mm/year, and in the northeastern region within Canada, where it ranges between 1,000 and 1,500 mm/yr. The semi-arid and arid regions of the southeast receive the least precipitation, ranging from 150 to 250 mm/yr. Mean annual precipitation within the modeled region is approximately 700 mm/yr.

The water resources of the CRB have been developed extensively since the early 1930's, beginning with the construction of Bonneville Dam in 1938. Thirty major federal dams have been constructed on the Columbia River and its tributaries in addition to several dozen non-federal dams. The dams serve a number of uses, including flood control, irrigation, electric power generation, fisheries protection and enhancement, recreation and water supply (USGS, 1994). In this study, naturalized streamflow data, which represent observed streamflow corrected for dam storage, dam evaporation and irrigation withdrawals, were used in place of observed streamflow records (see Chapter 3 for details on naturalized data). Thus, the effects of dams on streamflow were not evaluated.

2.2 Overview of human settlement in the Columbia River basin

The historical inhabitants of the Columbia River basin were the Native Americans. Unlike the earlier American Indians of pre-historic times, these people were not nomadic, but remained within favored regions where they could gather adequate supplies of food and other needs. Fire was used liberally for communicating with others and as a part of ceremonial and ritual events. The widespread use of fire was highly influential in shaping the vegetation prior to European settlement (Quigley and Arbelbide, 1996). These fires differed from fires ignited by lightning in their low intensity, high frequency and seasonality (Lewis, 1985). A result of the characteristic low intensity, high frequency fires was enriched forage for grazing and stimulation of vegetation and berry regrowth for human and animal consumption.

Euro-American interest in the U.S. portion of the basin began in the early 1800's with the travels of Lewis and Clark. The establishment of trading posts by fur trading companies was followed by the westward migration of families headed for the Willamette Valley in Oregon. In 1859, the discovery of gold in the northern Rockies marked the beginning of massive migration to the interior portion of the basin. Local economies developed around the mining industry, resulting in new territories being formed in Idaho and Montana and parallel development of the local timber industry. In turn, the development of towns and local economies drew farmers and stock raisers to the area. Wagon roads, steamboats and railroads were developed in the 1880's to link the west with

trade centers in the midwest and east.

By 1990, the population of the CRB had grown to approximately 2 million people, with the majority of the population residing in urban centers. The extent and effects of urbanization are discussed further in Section 2.2.4.

2.3 Land use and land cover changes

Anthropogenic activities in the CRB since the early 1900's, such as timber harvest, conversion of land for agriculture, livestock grazing, fire suppression and exclusion, introduction of exotic plant species and urbanization, have profoundly affected the vegetation. Changes in the extent and distribution of forest and rangeland vegetation, which have resulted from a combination of these anthropogenic activities and natural processes, are discussed below.

2.3.1 Forests

Forests continually undergo change through various combinations of natural disturbances, such as fire, climate change, insects and disease and anthropogenic disturbances such as timber harvest, roads and fire suppression policies. Today, forests cover approximately 55 percent of the total basin area. Figure 2.3 shows the spatial extent of forested areas.

2.3.1.1 Timber harvest

In the early 1900's, the northern interior Columbia basin became a major timber producer. Idaho saw more than a 10-fold increase in harvest between 1899 and 1910, with 745 million board feet of lumber sent to national markets by the end of the period. Early harvest was focused on large ponderosa pine and western larch, accomplished with select cutting practices. Growth of the timber industry continued for several decades, spurred by the growth of urban cities in the Midwest and California. Technology, such as skidders, caterpillar tractors, log trucks and chain saws dramatically lowered costs and improved productivity. In 1993, approximately 1,610 million board feet were harvested in Montana and Idaho (Warren, 1996) and 1,022 million board feet were harvested in eastern Washington (Larsen and Gobroski, 1995), with the majority taken from private lands and roughly 15 percent taken from national forests. In the interior portion of British Columbia, approximately 21 million board feet of timber were harvested in 1995 (Warren, 1996).

The hydrological effects of forest harvest have been heavily investigated since the 1950's. Rothacher (1970) found that clear-cutting and the construction of forest roads increase peak discharge following small, early wet season storms. Jones and Grant (1996) found that road construction combined with patch clear-cutting over 10 to 25 percent of the basin area caused substantial long-term increases in peak discharges for large and small basins in the Western Cascades.

Since 1900, timber harvested from federal lands in the western U.S. have declined, while harvest in Canada and other parts of the U.S. has increased. Timber harvest in the basin area currently comprises 10% of the total national harvest, which represents a decline from 17% in 1986. It is expected to continue declining to about 5% by the year 2000 (Quigley and Arbelbide, 1996).

2.3.1.2 Dry forest

The term "dry forest" applies to forests which occur at high-elevation (typically above 4,000 ft.) and are subject to drought and moisture limitations. Within the U.S. portion of the CRB, dry forests are located primarily in central Idaho and western Montana. Vegetation types found within these areas include Douglas-fir, ponderosa pine, grand fir and white fir.

The spatial extent of dry forests across the CRB has changed drastically as a result of anthropogenic activity since the 1800's, from open stands of large trees mixed with clumps of small trees to more densely packed younger stands with multiple canopy layers. The area dominated by shade-tolerant trees is now nearly double what existed prior to Euro-American settlement. Dry forest areas most significantly affected are those which have been roaded and harvested (Quigley and Arbelbide, 1996). Large ponderosa pine trees were selectively logged, leaving behind smaller, perhaps genetically inferior trees, such as Douglas-fir. Fire exclusion policies encouraged the growth of densely packed

shade-tolerant trees in place of open, park-like stands. Lack of frequent, low intensity fires reduced stand thinning and eventually increased competition for sunlight and nutrients. Changes in the condition of CRB dry forests include loss of growth potential due to overstocking, higher risk of severe insect, disease and fire problems and loss of forest habitat space with respect to pre-settlement conditions.

2.3.1.3 Moist forest

Moist forests within the U.S. portion of the CRB consist of cedar, hemlock, Douglas-fir, grand fir and spruce-fir. They generally occur in areas of transition between drier, lower elevation forests and higher elevation subalpine forests (Agee, 1993) within northeastern Washington, northern and central Idaho and western Montana.

As in the case of dry forests, moist forests within roaded and harvested areas have been changed most significantly from their condition prior to Euro-American settlement. Selective harvest of shade-intolerant species, such as western larch, western white pine and ponderosa pine, resulted in dominance of shade-tolerant species associated with poor form and/or growth. Much of the moist forested area has become more sensitive to root diseases as a result of fire exclusion, selective harvest of shade-intolerant species and the spread of Douglas fir and true firs in dense, multi-layer stands (Hessburg and Smith, 1996). White pine blister rust has affected at least 50% of the moist forest areas.

2.3.1.4 Cold forests

Cold forest vegetation types within the U.S. portion of the basin consist of mountain hemlock, spruce-fir, aspen, whitebark pine and alpine larch. They are sparsely located within cold, subalpine regions of central Idaho and southwestern Montana. Growth of cold forests is limited primarily by a short growing season and, in some cases, by low available moisture.

The effects of anthropogenic activities, such as fire suppression, timber harvest, road construction and livestock grazing, are less apparent in cold forests than in dry and moist forests. Loss of whitebark pine due to blister rust and harvest of old multi-layer forest have affected the structural composition in some regions. However, inherently longer fire intervals and slow rate of natural change in vegetation associated with the cold climate have helped mitigate changes.

2.3.2 Rangeland

Rangelands are non-forested areas which contain grasses, shrubs, sparsely wooded areas and riparian areas around water. Since the 1900's, livestock grazing, fire suppression efforts and the introduction of non-native plants in combination with changes in climate and soil have caused extensive change to rangeland vegetation. Figure 2.3 shows the spatial extent of range vegetation within the CRB.

2.3.2.1 Livestock grazing

Historically, ungulates (large mammals with split hooves) such as deer, elk, mountain sheep, antelope and bison lived in eastern Washington and Oregon. A predator-prey balance kept the ungulate population stable. The ungulates were highly mobile, with their grazing and browsing dependent upon vegetation cycles and seasonal weather patterns. Accordingly, low elevation valleys were grazed during winter. In spring, the herbivores would move to higher elevations for herbaceous vegetation, allowing the vegetation to regrow in the valleys and fuels for summer fires to accumulate. The cycle was complete with the return of the animals to lower elevations in fall (Leonard and Karl, 1995). Bunchgrass and the native grasses which they consumed were stimulated by the disturbance, resulting in a higher abundance of plants (Haynes and Horne, 1996).

The introduction of livestock in the 1860's and rapid expansion of the livestock industry throughout the late 1800's created new pressures to range vegetation. Livestock are sedentary animals and will remain in place for as long as food, water and other supplies are available. Thus, the historical seasonality in the grazing cycle changed to a pattern of year round, open range grazing. Hydrological consequences of overgrazing include reduced infiltration and increased water yield. Naeth et al. (1990) examined the effects of grazing intensity on infiltration for several plots of mixed prairie and fescue grasslands in the foothills of Alberta, Canada. They found that steady state infiltration was 1.5 -2.0 times higher for lightly grazed land than for moderately, highly or very highly grazed land. Fuls et al. (1992) reported increased soil compaction, loss of topsoil, a 60 percent

reduction in soil moisture content and 90 percent reduction in basal vegetation resulting from patch-overgrazing in the grasslands of southern Africa. In the CRB, several decades of overgrazing have affected streams and riparian vegetation in eastern Oregon and Washington, fostered the spread of non-native annual plants, such as cheatgrasses, and facilitated a reduction in fire frequency.

2.3.2.2 Fire regimes

Fire frequency within rangelands has been reduced, mostly due to fire suppression efforts and livestock grazing removal of fuel, while the intensity of rangeland fires and occurrence of lethal fires has significantly increased. Lethal, or stand-replacing, fires are defined for forests as fires which remove more than 20 percent of the basal area or 10 percent of the canopy cover. For rangelands, the term lethal is applied to fires which destroy most of the shrub overstory (Quigley and Arbelbide, 1996). Fire suppression practices are associated with the invasion of conifers into previously non-forested regions, increased tree density in former savanna-like stands of juniper and ponderosa pine, and dominance of big sagebrush and other shrubs with the loss of herbaceous vegetation and native annual grasses. The first of these effects, invasion of rangeland by conifers, has resulted in disruption of soil and nutrient cycling and reduced soil cover, allowing for increased erosion.

Fire frequency actually increased in some areas with respect to historical frequency

(Quigley and Arbelbide, 1996). This is true mostly in drier locations where exotic annual grasses, such as cheatgrass, have been introduced. The exotic annual grasses provide fuel for frequent, low intensity fires, which help perpetuate the dominance of these grasses through competition with native species.

2.3.2.3 Introduction of exotic plants

Exotic, or non-native, plants in the CRB include noxious weeds and non-native annuals. According to the Federal Noxious Weed Act, the term “noxious weed” applies to non-native weed species which cause disease or are associated with adverse impacts on agriculture, commerce in the U.S., or public health. Common varieties of noxious weeds found within CRB rangelands include bull thistle, Canada thistle, dalmation toadflax, diffuse knapweed, hoary cress, leafy spurge, musk thistle, Russian knapweed, Scotch thistle, spotted knapweed, yellow starthistle and yellow toadflax (Leonard and Karl, 1995). Seeds for these exotic plants were introduced to the rangelands with the beginning of agriculture and livestock grazing. Throughout the 1990’s, noxious weeds have continued to spread rapidly over most of the basin, aided by soil disturbance and prolific seed production. Vehicles, wind, wildlife, livestock, water, machinery and pack animals help distribute the seeds over long distances. Once established, noxious weeds outcompete native species for available nutrients and water and increase rangeland fire frequency. Invasion by noxious weeds results in a reduction in diversity and abundance of

native vegetation, reduced forage, degradation of wildlife habitat, increased soil erosion and decreased water quality.

Decades of overgrazing of perennial grasses and forbs (commonly referred to as weeds or wild flowers) has led to widespread invasion by non-native annual grasses, such as cheatgrass, medusahead, Russian thistle and mustards in the U.S. portion of the CRB. These annual grasses typically change fire frequency from a 25-100 year return interval to a five year return interval (Quigley and Arbelbide, 1996). The increased fire frequency, in combination with continued overgrazing, promotes and perpetuates dominance of the non-native annuals grasses over native species. Cheatgrass is an especially problematic annual grass which has spread extensively through most of the basin's rangelands, particularly in the regions of the Columbia Plateau and Owyhee uplands (Pellant, 1995). It was likely introduced in the 1890's by contaminated grains from Europe. Frequent fires resulting from dominance of large areas by cheatgrass has caused degradation of wildlife habitat, threatened the survival of sensitive native species, reduced plant diversity and native plant abundance and extended recovery periods for the land after burning (Quigley and Arbelbide, 1996).

The most highly affected native vegetation communities include dry grasses and shrubs (Agropyron Bunchgrass, Fescue-Bunchgrass, Antelope Bitterbrush, Bluebunch Wheatgrass) and riparian herbs and shrubs. Noxious weed control has had little effect due primarily to budget constraints of the local, state and federal agencies concerned with weed management. One course of action has been the introduction of forage grasses

(Miles and Karl, 1995) to counter the soil, hydrologic and nutrient effects resulting from removal of vegetative cover. The problem associated with this technique is that biodiversity is reduced, especially when vegetation was removed by fire, grazing or cultural practices before seeding of forage grasses.

2.3.3 Urbanization

The extent of urbanization within the CRB is small, especially in the Canadian portion of the basin. Figure 2.3 shows the locations of urban cities within the U.S., including Spokane and Yakima in Washington, Boise, Idaho, Bend, Oregon and Missoula, Montana.

The dominant hydrological effect of urbanization is reduced infiltration due to increased impervious surface. Ferguson (1990) found that runoff was increased in wet years as a result of urbanization in a gauged watershed in Atlanta, Ga.. During dry years, however, total runoff decreased in comparison to the pre-urbanization period, which he attributed to advectively assisted urban evaporation.

Within the CRB, expansion of urban areas has caused a reduction in rangeland vegetation, such as grasses, shrubs and riparian species (Quigley and Arbelbide, 1996). Furthermore, the expansion of urban areas into or adjacent to rangelands has intensified the demand for fire suppression efforts in the vicinity of the major urban centers.

2.3.4 Agriculture

Agriculture in the CRB is concentrated in the southeastern and central portions of the basin, with minimal coverage in the Canadian portion of the basin (Loveland et al., 1991). Figure 2.3 shows the spatial extent of agricultural coverage. In eastern Washington, northeastern Oregon and southern Idaho, primary crops include wheat, apples, alfalfa, potatoes, peas, corn and grapes.

Irrigation has been an essential aspect in the growth of agricultural activity in the CRB. Approximately 6 percent of the Columbia River's mean annual runoff is diverted to irrigate 7.8 million acres of land (USGS, 1994). Some of the diverted water (perhaps as much as half) eventually returns to the river, so this value represents an upper bound on consumptive use by agriculture. The federal Columbia Basin Project, for instance, uses water from Grand Coulee Dam to irrigate approximately 500,000 acres of farmland in the desert-like terrain of central Washington. Irrigation activity is especially intense on the Snake River plain. The Minidoka Project, for instance, uses thousands of miles of distribution canals to irrigate over one million acres of farmland.

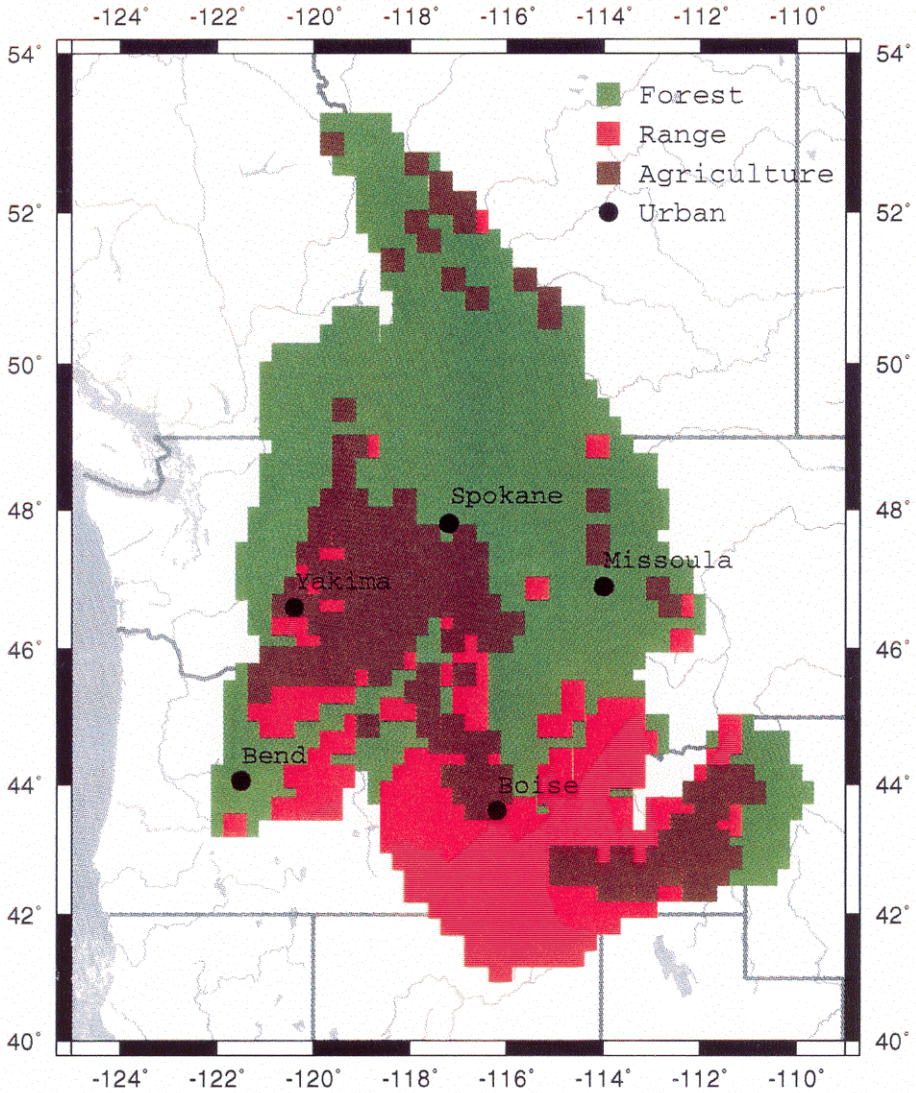


Figure 2.3 Location of forested, rangeland, agricultural and urban areas within the Columbia River basin.

3. Model components

This chapter discusses the modeling approach used to simulate streamflow. The models used, in sequence, are the National Weather Service River Forecast System (NWSRF) snow accumulation/ablation model, the Variable Infiltration Capacity - 2 Layer (VIC-2L) hydrologic model and a linear routing model. Figure 3.1 shows the schematic sequence in which the model components were implemented.

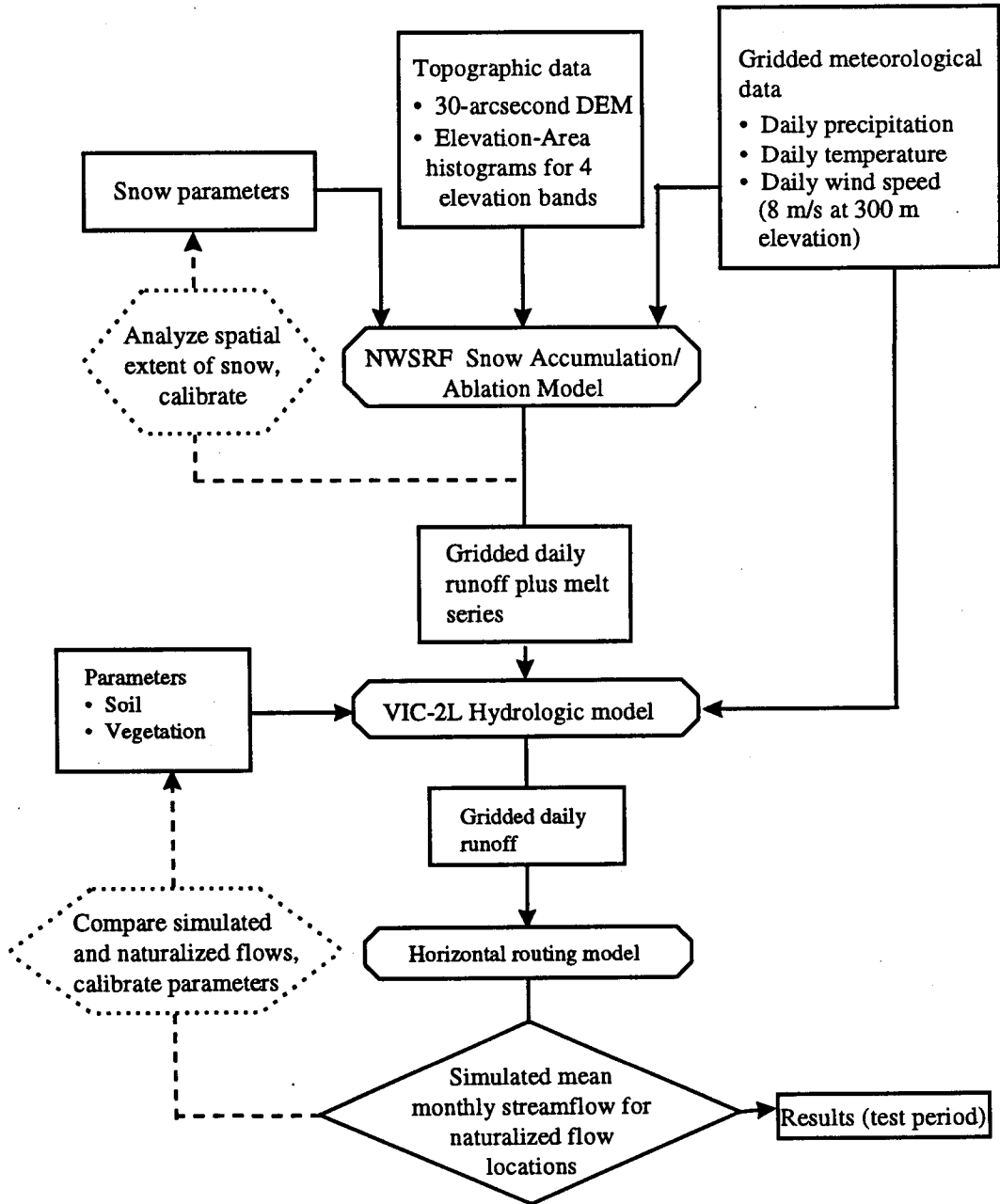


Figure 3.1 Schematic modeling approach.

3.1 Snow Ablation/Accumulation Model

A temperature index ablation/accumulation model is used to compute the energy exchange at the snowpack/atmosphere interface (Anderson, 1973). Air temperature is the sole index for determining the form and temperature of precipitation and the terms of the energy budget used in calculating melt during rain periods. Snowpack surface heat content, surface temperature, surface layer melt and liquid water content are accounted for continuously.

Melt is computed using one of two formulas, depending primarily on the occurrence of rainfall. During periods of rain, the change in snowpack heat content is calculated using a simplified energy budget. During non-rain conditions, including snowfall, change in snowpack heat content is taken as the difference between air temperature and base temperature (0°C in this application) scaled by a seasonally varying melt factor (see Anderson, 1973 for details).

Model inputs are daily precipitation and maximum and minimum air temperature. The model operates on a 6-hourly time step in order to represent the diurnal melt cycle. Thus, temperature is interpolated to 6-hourly values using daily maximum and minimum temperature. Daily precipitation is partitioned uniformly to the six hour periods.

The model resolves sub-grid orographic precipitation effects and temperature lapsing in mountainous regions by allowing for an arbitrary number of elevation bands within each grid cell. Elevation bands are determined by elevation-area histograms

computed from a Digital Elevation Model (DEM) at much finer resolution than the model grid mesh. The specification of the four elevation bands used in this application was based on area-elevation curves derived from a 30-arcsecond DEM. Temperature was lapsed linearly to each of the bands using a lapse rate of $6^{\circ}\text{C}/\text{km}$. Precipitation was lapsed to the band elevations using relationships inferred from Precipitation Regression on Independent Slopes Model (Daly et al., 1994). The rain plus melt series output by the snow model was aggregated to a daily time step and used as the effective precipitation input to the VIC-2L model.

3.2 VIC-2L Land Surface Model

The VIC-2L is a land surface hydrology model which represents sub-grid variability in soil moisture and infiltration capacity. The VIC-2L can be coupled on-line with atmospheric models or run off-line in water balance mode. In the former mode, the GCM provides hydrological and meteorological forcings to the VIC-2L, which solves energy balance equations to partition energy and water fluxes between the soil, vegetation and atmosphere. In the water balance mode, VIC-2L is forced by an off-line daily effective precipitation series. Water fluxes are partitioned into daily evaporation, baseflow, surface runoff and soil moisture series. The daily runoff and baseflow are summed and retained for post-processing by a routing model. In this step, grid cell runoff is spatially integrated to simulate streamflow at selected naturalized streamflow locations.

Simulated daily streamflows are aggregated to a monthly time step and averaged over all years of the simulation to produce long-term monthly means. The simulated long-term monthly means are compared with mean monthly naturalized flows at corresponding locations during calibration and testing.

Sub-grid soil moisture and infiltration capacity are related to percent grid cell surface area saturated, using a formulation included in the Xinanjiang model of Zhao *et al.* (1980). A single parameter, b_i , determines the shape of the infiltration capacity curve. Direct runoff (Q_d) is calculated as precipitation in excess of infiltration capacity:

$$Q_d = P + W_o - W_o^{\max} \quad I_o + P \geq I_m \quad (1)$$

or

$$Q_d = P + W_o - W_o^{\max} (1 - (1 - (I_o + P)/I_m)^{1/b_i}) \quad I_o + P < I_m \quad (2)$$

where subgrid infiltration capacity is calculated as:

$$I = I_m (1 - (1 - A_s)^{1/b_i}) \quad (3)$$

and P is precipitation, W_o is soil water content prior to a precipitation event, W_o^{\max} is the maximum water content of the upper layer, I_o is the saturation infiltration capacity, I_m is the maximum infiltration capacity and A_s is the saturated fraction of the grid-cell.

Baseflow is represented as a nonlinear recession following the Arno model of Francini and Pacciani (1991) and is calculated as:

$$Q_b = k_1 * W_2 \quad W_2 \leq W_s * W_2^{\max} \quad (4)$$

or

$$Q_b = k_1 * W_2 + k_2 * (W_2 - W_s * W_2^{\max})^{k_3} \quad W_2 > W_s * W_2^{\max} \quad (5)$$

where W_2 is the soil moisture in the second soil layer, k_1 is the linear storage constant for the linear baseflow portion and $\ln(2/k_1)$ is the half time decay of the second layer. The remaining variables are used to represent the nonlinear portion of the baseflow. k_2 is the nonlinear baseflow storage coefficient and the value k_3 determines the linearity or non-linearity of Equation 5.

Drainage (Q_{12}) from the upper soil layer to the lower is calculated as:

$$Q_{12} = K_s(W_o - \theta_r)/(W_o^{\max} - \theta_r)^{2/B_p+3} \quad (6)$$

where K_s is saturated hydraulic conductivity, θ_r is residual water content (set to zero), and B_p is the pore distribution index (Lohmann *et al.*, 1996).

Evapotranspiration is calculated separately for each vegetation class and for bare soil. Transpiration is formulated by the Penman-Monteith equation, which requires input net radiation, vapor pressure deficit, aerodynamic resistance, minimum stomatal resistance,

architectural resistance, leaf area index (LAI), soil moisture stress factor, air temperature (used to calculate the slope of the saturated vapor pressure deficit curve), and elevation. In this application, LAI was allowed to vary monthly for forest and agriculture.

Architectural resistance represents the aerodynamic resistance between the leaves and the canopy top associated with imperfect canopy ventilation and is a function of vegetation cover type (Ducoudre et al., 1993).

Evaporation from bare soil is calculated using the Arno model (Francini and Pacciani, 1991) for the upper soil layer at the potential rate for the saturated area. Bare soil evaporation from the unsaturated area is computed as a fraction of the potential rate, where the fraction is a function of percent grid cell area saturated (A_s) and the infiltration curve shape parameter, b_i . Total bare soil evaporation is formulated as:

$$E = E_p \times \left[\int_0^{A_s} dA + \int_{A_s}^1 \frac{i_o}{A_s^{i_m} [1 - (1 - A)^{1/b_i}]} dA \right] \quad (7)$$

where the first term represents saturated bare soil evaporation and the second represents evaporation from unsaturated soils. The solution to the second term is approximated as a power series expansion following Liang et al. (1994). Total daily grid cell evaporation is computed as the areally weighted sum of evaporation from each vegetation class and bare soil.

3.3 Routing Model

The routing model of Lohmann et al. (1996) was used. It is forced by grid cell runoff (direct runoff plus baseflow) production from the center of each grid cell and predicts streamflow at specified grid-cell outlets using a user-defined channel network. Runoff is separated into two time scales, fast and slow flows, to represent the spectral time response of streamflow to precipitation events. The two components are related:

$$dQ^s(t)/dt = -k*Q^s(t) + b*Q^f(t) \quad (8)$$

where $Q^s(t)$ is slow flow and $Q^f(t)$ is fast flow. The slow and fast components sum to the total simulated discharge, where fast flow is analogous to direct runoff and slow flow is analogous to baseflow. Fast flow is calculated as:

$$Q^f(t) = \int UH^F(t)P^{eff}(t-\tau)d\tau \quad (9)$$

where $UH^F(t)$ is the impulse response function for the fast flow (similar to the time required for discharge from one cell to travel to the gauging station) and P^{eff} is the portion of precipitation converted to streamflow, assuming there is a linear relationship between actual precipitation and P^{eff} . Lohmann et al. (1996) provide the complete solution to

Equations 8 and 9. Total flow is routed linearly:

$$\delta Q/\delta t = D\delta^2 Q/\delta x^2 - C\delta Q/\delta x \quad (10)$$

where D and C coefficients are diffusion and velocity, respectively.

Inputs to the routing model include a flow direction network, internal unit hydrographs, reservoir information and gridded diffusion and velocity estimates. The flow direction network was prepared by manually tracing high resolution maps of streams and tributaries in the Columbia basin to a quarter-degree basin mask, allowing only one direction of flow for each grid cell. For cells where the flow direction could not be determined from the map, the outlet was assigned using a steepest descent algorithm and digital elevation data. A mask of integer values, ranging from 1 to 8, with 1 indicating northward and 3 eastward, etc., is the ultimate representation of the channel network which is input to the model. Figure 3.2 shows a schematic representation of the routing network used in this study. Velocity was held constant at 1 m/s and diffusivity at 1,000 m²/s globally following Lohmann et al. (1996).

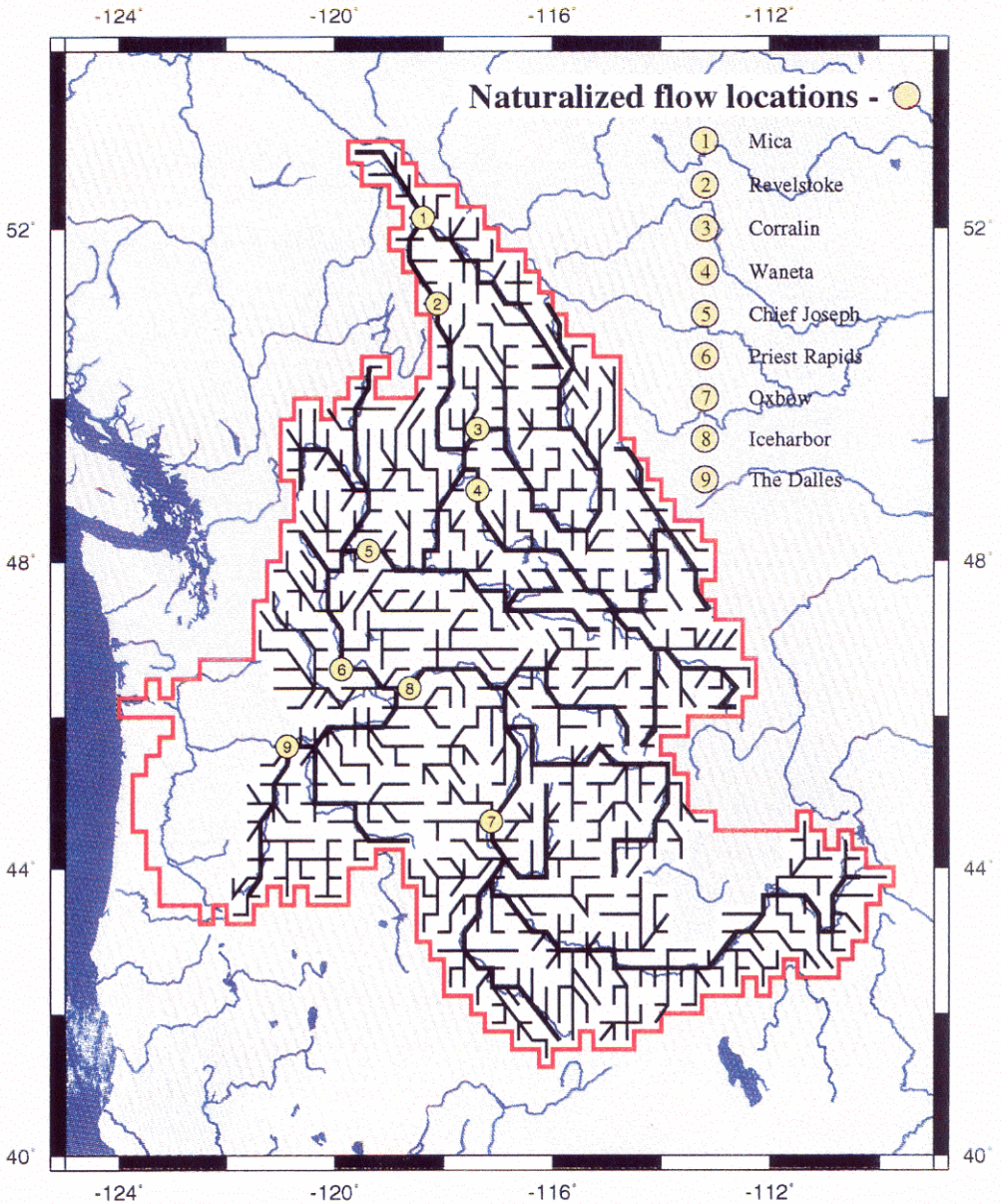


Figure 3.2 Flow direction network input to the routing model.

Reservoir capacity and minimum release rates can be specified in the model to account for the effects of dams. However, since naturalized flows were ultimately used in this study to compare simulated streamflow, reservoir capacities were set to zero. The naturalized flow records represent observed flow before the construction of major dams and agricultural withdraws (circa 1928). They are derived from modified flows representing streamflow at the 1990 level of water resources development. Crook (1993) constructed the modified flows as follows:

$$\text{Modified flow} = \text{Observed flow} + \Delta\text{Storage} + (\text{Historical Evap.} - \text{Dam Evap.}) + (\text{Historical Withdrawals} - 1990 \text{ Withdrawals}) \quad (11)$$

where $\Delta\text{Storage}$ is measured. Naturalized flows were obtained by adding dam evaporation and 1990 withdrawals to the modified flow records. Data for historical withdrawals and historical evaporation were limited, making the reliability of the above calculation subject to best estimates of these terms. Since no major dams were constructed and agricultural withdrawals were minimal in 1928, historical evaporation and withdrawals were set to zero.

For the Upper Snake basin, lack of data for 1990 net withdrawals made the above method infeasible. Instead, regulated flows representing 1990 level of development were used for comparing simulated streamflow in this region. These records were constructed by adding a correction (the difference between historical flows and regulated flows at

1990 level of development) to regulated 1990 flows.

4. Model implementation

This chapter describes the application of the VIC-2L hydrologic model in water balance mode at quarter-degree resolution for the region of the Columbia River basin upstream of The Dalles. Data selection, gridding of meteorological data and parameter specification are discussed.

4.1 Input data

The VIC-2L model requires daily meteorological forcings, including precipitation, maximum and minimum air temperature and wind speed. Other daily meteorological values, such as net radiation and vapor pressure deficit, are calculated on-line as a function of the input diurnal temperature range (see Section 4.1.2 for details)

4.1.1 Digital elevation model

A 30-arcsecond digital elevation model was used to represent the topography of the basin. Average elevations were calculated for quarter-degree grid cells and for four elevation bands as required by the snowmelt model. Mean band elevation was used to lapse temperature and precipitation in the snow model, while mean grid cell elevation was used to lapse temperature from station to cell elevation in the meteorological data gridding process.

4.1.2 Meteorological data

Meteorological data requirements for the VIC-2L (water balance mode) include precipitation, maximum and minimum air temperature and daily wind speed at given elevation. Net radiation and vapor pressure deficit are not input directly in water balance mode, but rather are parameterized internally as a function of daily maximum and minimum temperature. Most of the precipitation and temperature data were obtained from Wallis et al. (1991). Whenever possible, grid cells with less than two stations meeting the selection criteria (listed below) were augmented with data from Earthinfo Inc. (1991). Meteorological data for Canada were provided by Atmospheric Environment Canada. Approximately 300 stations were used in total. Criteria for selecting precipitation and temperature stations included:

1. Station must have been in continuous operation from January, 1980 - September, 1995.
2. Station elevation should not have changed by more than 50 ft during the same period.
3. Station location should not have changed by more than one-half mile during the same period.

4. Record should be at least 85% complete during the same period.

Figure 4.1 shows the spatial distribution of meteorological stations for the basin. Stations with sufficient length of record were sparse in the northern portion of the basin, resulting in a density of approximately 1 station for every 30 grid cells.

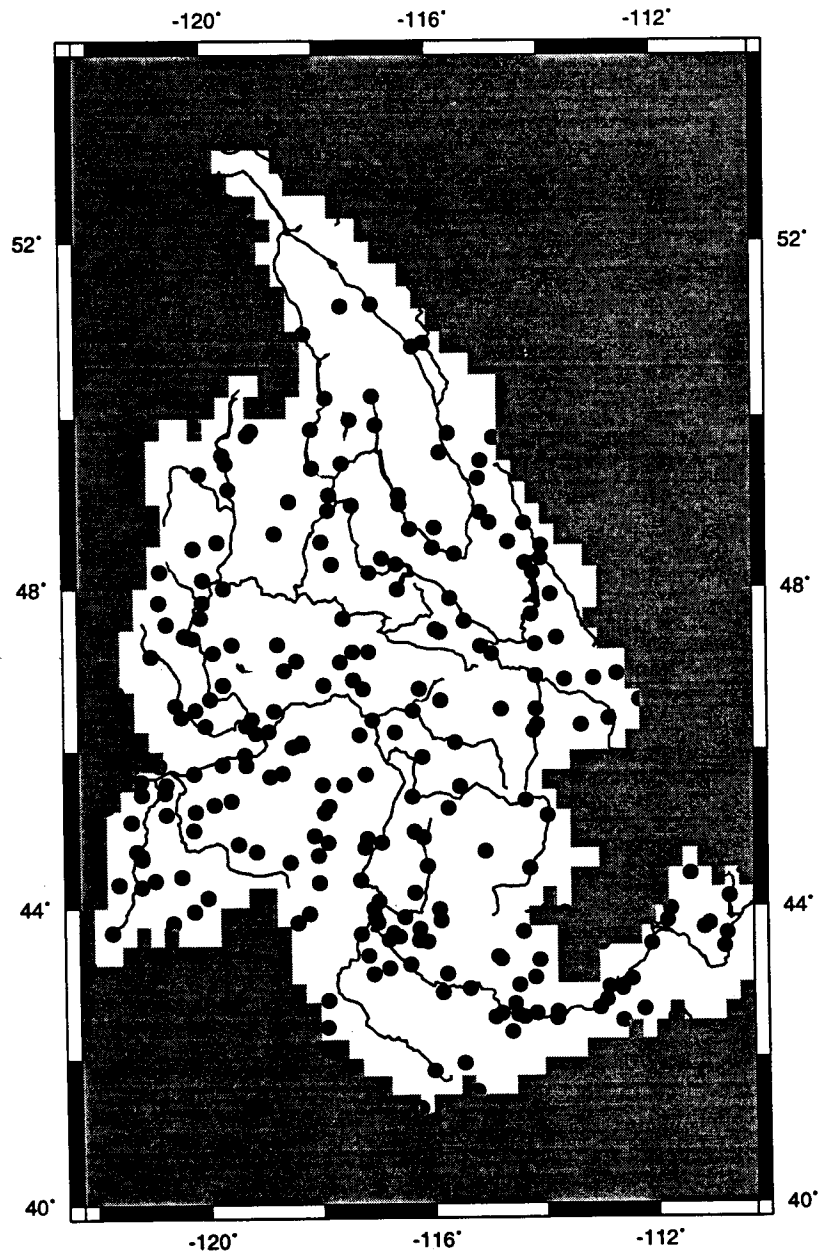


Figure 4.1 Location of precipitation and temperature data stations.

Station precipitation data were interpolated to the model grid mesh using an inverse distance squared weighting factor applied to four nearest neighbors. This step produced a gridded daily time series of precipitation. Because precipitation has a considerable degree of spatial variability, especially in regions of complex terrain, the precipitation monthly means were adjusted at each grid cell to reduce long term bias. This was accomplished by normalizing the gridded daily fields by the grid-cell long term monthly mean, resulting with a global long term monthly mean of 1.0. The normalized daily series for each grid cell were then scaled by a monthly adjustment factor.

Daly et al. (1994) present an approach, termed PRISM (Precipitation Regression on Independent Slopes Model), to areally estimate mean monthly precipitation for mountainous regions to resolve the small-scale spatial heterogeneities associated with complex topography. The PRISM mean fields at 2.5-minute resolution were obtained by combining data from approximately 8,000 precipitation stations within the CRB with DEM data at 2.5-minute resolution. The DEM was used to delineate regions of equal slope orientation for which independent slope-precipitation regression relationships were derived. These regression relationships were then used to estimate precipitation for pixels where station data were lacking (Daly et al., 1994). The monthly PRISM means were averaged for each quarter-degree grid cell and used to scale the normalized gridded daily fields. The spatially interpolated and gridded precipitation data were adjusted to have the PRISM means for each quarter degree grid cell.

Temperature was gridded at quarter-degree resolution using an inverse distance squared weighting factor applied to four nearest neighbors. A lapse rate of 6°C/km was used to lapse temperatures from the station elevation to the mean grid cell elevation.

A global wind speed of 8 m/s at 300 m elevation was used. The VIC-2L internally adjusts the 300 m wind to the surface using an assumed logarithmic wind profile.

In water balance mode, the VIC-2L parameterizes vapor pressure deficit and net radiation as a function of mean and minimum daily air temperature. Dew point temperature is approximated as minimum air temperature for computing daily vapor pressure deficit, D :

$$D = e_s(T_{\text{air}}) - e_s(T_{\text{min}}) \quad (15)$$

Net radiation is calculated as a function of potential radiation at the top of the atmosphere (Shuttleworth, 1993), which is attenuated through the atmosphere as a function of atmospheric transmissivity, τ :

$$\tau = A[1 - \exp(B\Delta T^c)] \quad (16)$$




where ΔT is the difference between maximum and minimum air temperature, A is the maximum clear sky transmissivity and B and C are empirical constants taken from Bristow and Campbell (1984).

4.2 Parameter estimation

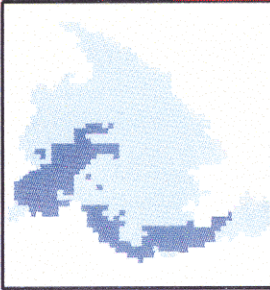
Parameters were estimated at the quarter degree model resolution for the snowmelt and VIC-2L models. The VIC-2L requires soil and vegetation parameters which generally apply to canopy conductance, aerodynamic resistance and soil and vegetation water holding capacity.

4.2.1 Snow Model Parameters

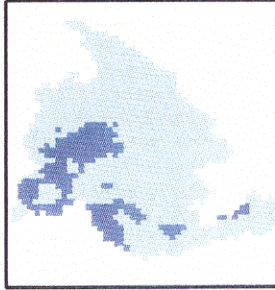
The reader is referred to Anderson (1973) for a detailed description of the snow parameters. Most of the parameters remained unchanged from their values suggested by Anderson for the Columbia basin (see Sias et al., 1994, for a listing of parameter names and values). Approximate calibration of maximum and minimum melt factors for the U.S. part of the CRB was based on initial estimates at one-degree resolution from Nijssen et al. (1997) and comparisons of simulated and observed snow extent (Figures 4.2 and 4.3) for several days between January 1st and June 30th spanning years 1990 through 1994. The melt factors are seasonally varying with a maximum in June, minimum in January and sinusoidal variation throughout the year.

-  - Snow
-  - No snow
-  - No data

Jan 20, 1994



Jan 30, 1994



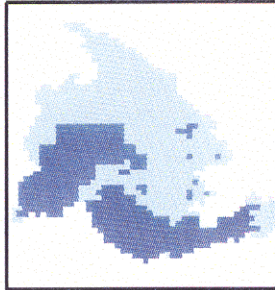
Feb 3, 1992



Mar 15, 1994



Mar 27, 1994



Apr 16, 1994



May 3, 1994



May 6, 1994



Jun 13, 1993

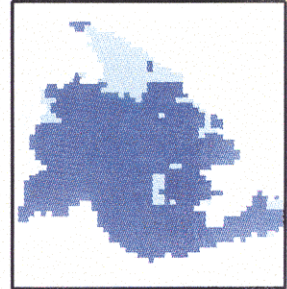


Figure 4.2 Simulated snow areal extent.

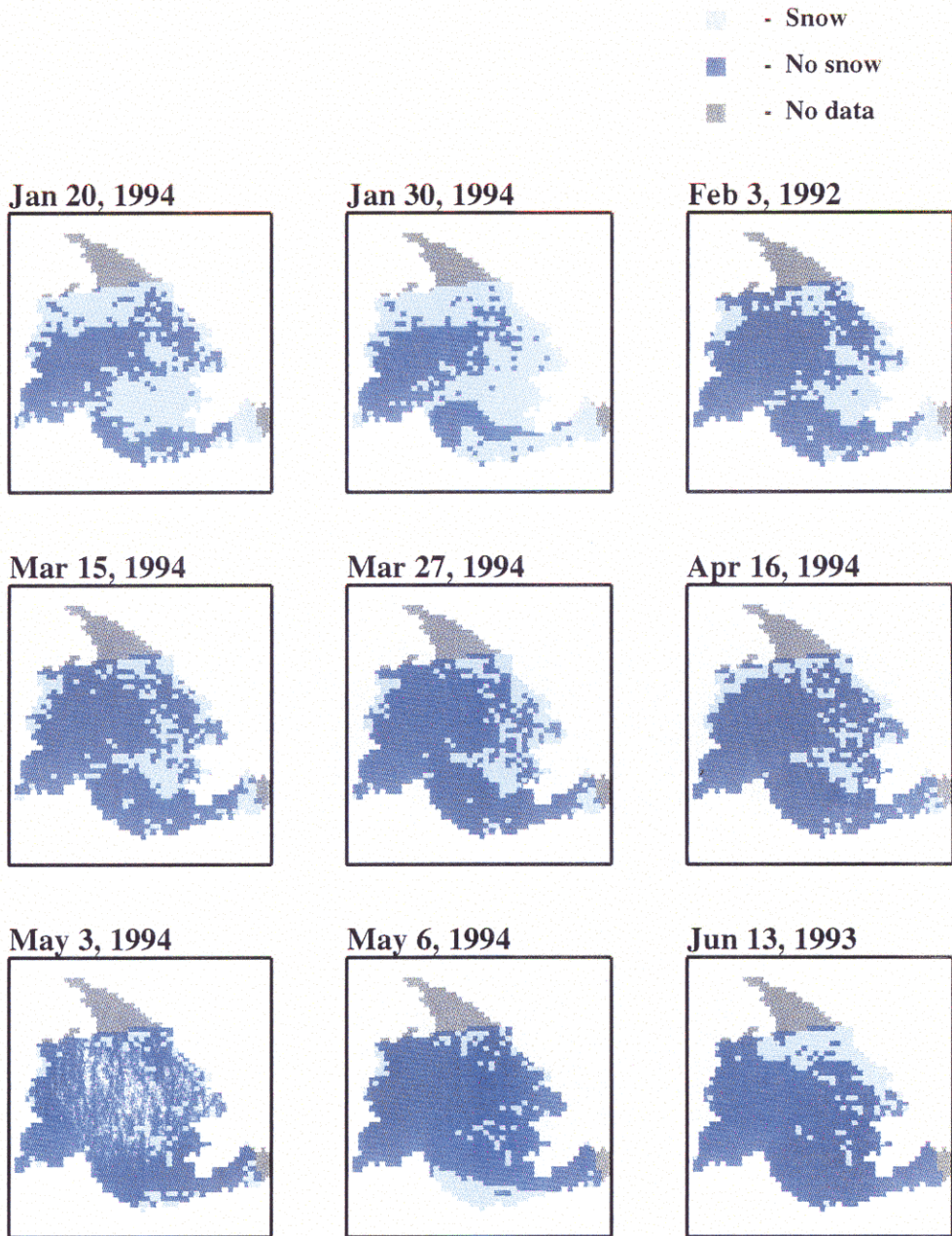


Figure 4.3 Snow areal extent observed by GOES satellite.

The range of calibrated maximum and minimum melt factors varied from 3.0 mm/day to 7.2 mm/day and 0.8 mm/day to 4.0 mm/day, respectively, with values increasing southward. Other important parameters include S_i , which is the mean areal water equivalent above which there is always 100 percent snow cover. Maximum S_i of 450 mm was assigned at the northern-most latitude with values decreasing southward to 100 mm, following Anderson. The gauge catch deficiency factor, SCF, which scales precipitation to account for snow catch deficiency, was set globally to 1.0, since PRISM data were used to spatially rescale mean monthly precipitation.

An evaluation of the snow model predictions was performed using satellite imagery of snow areal extent obtained from NOAA's National Operational Hydrologic Remote Sensing Center. In the comparison of snow extent, grid cells with simulated values of total water equivalent (TWE) averaged over the four elevation bands greater than zero had snow and the remaining cells had no snow. The observed images were derived from GOES satellite data from 1990 to 1995, covering approximately 90% of the basin (NOAA, 1990-1995). The data depict each pixel by an integer value indicating the presence or absence of snow or cloudiness (no information regarding snow cover). Data for nine days were ultimately used for comparison, where minimal cloudiness and time of year (between January and August) were the basis for selection. The GOES data were aggregated from 1-km to quarter-degree using the modal value. Unfortunately, most of the Canadian region, where snow melt is highly important to the timing of peak streamflow, is not within the extent of the NOAA archives. Nonetheless, Figures 4.2 and

4.3 show approximate agreement between simulated and observed snow extent for the winter and spring days. Some overprediction of snow coverage within the northeastern region of the depicted area during early spring is indicated.

Discrepancies in the comparison between the GOES satellite images and model predictions may be attributed to the inability of the GOES satellite to detect snow stored underneath vegetation canopies. Furthermore, the snowmelt model does not account for vegetation nor sublimation. Therefore, model predicted timing of spring snowmelt may be slightly underestimated, especially in the northern and northeastern regions where forest stands dominate the landscape.

4.2.2 Soil parameters

The VIC-2L model requires specification of seven soil parameters, including an infiltration capacity curve shape factor, b_i , total soil moisture storage capacity in both layers, $W_{c,tot}$, the fraction of total soil moisture stored in the bottom model layer, $W_{2/1}$, the maximum baseflow parameter, D_m , fraction of the maximum baseflow parameter, D_s , the fraction of maximum soil moisture at which the baseflow computation becomes nonlinear, W_s and saturated hydraulic conductivity, K_s . Initial estimates for all soil parameters were taken from a combination of sources, including soil characteristics data bases for the U.S. and relevant literature. The parameters were manually adjusted to obtain the final calibration, where the ultimate goal of the calibration was to reduce

computed long-term bias between simulated and naturalized mean seasonal and annual flows. The formulation of long-term bias is shown in Equation (19), in Section 4.5.

Initial estimates of K_s and $W_{c,tot}$ for the U.S. were derived from USDA STATSGO (State Soil Geographic data base) global soil classes data. The STATSGO data contain soil class designations for 11 fixed depth soil layers at 1-km spatial resolution. Table 4.1 shows the depth of each STATSGO soil layer.

Table 4.1 Depths of eleven STATSGO soil layers.

Layer number	1	2	3	4	5	6	7	8	9	10	11
Depth (mm)	50	50	100	100	100	200	200	200	500	500	500

For each STATSGO soil type, a mean porosity and saturated hydraulic conductivity were assigned following Rawls et al. (1992). Table 4.2 shows the porosity and saturated hydraulic conductivity associated with each soil type.

Table 4.2 Porosity and saturated hydraulic conductivity as a function of soil type^a.

STATSGO soil type	Description	Porosity	Ks (cm/hr)
1	Sand	0.437	23.56
2	Loamy sand	0.437	5.98
3	Sandy loam	0.453	2.18
4	Silt loam	0.501	0.68
5	Loam	0.463	1.32
6	Sandy clay loam	0.398	0.30
7	Silty clay loam	0.471	0.20
8	Clay loam	0.464	0.20
9	Sandy clay	0.430	0.12
10	Silty clay	0.479	0.10
11	Clay	0.475	0.06

^a Taken from Rawls et al. (1992).

Saturated hydraulic conductivity at 1-km resolution was calculated as the vertically weighted average saturated hydraulic conductivity for each STATSGO soil layer.

$W_{c,tot}$ was found as the sum over all layers of the product of depth and porosity:

$$W_{c,tot} = \sum_{n=1}^{n=12} (D_n * \Phi_n) \quad (17)$$

where, ϕ_n and D_n are porosity and depth of layer n , respectively. The values for K_s and $W_{c,tot}$ at 1-km resolution were averaged within quarter-degree blocks to obtain initial estimates for these parameters over the model grid mesh. Figure 4.4 shows the spatial distribution of K_s and $W_{c,tot}$ obtained by this method.

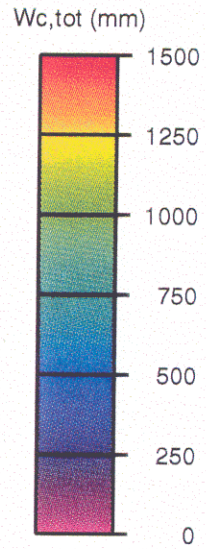
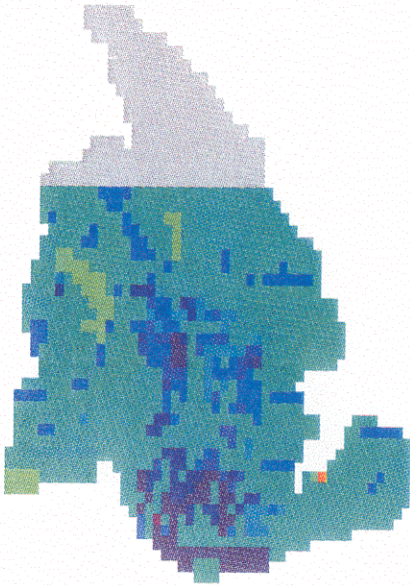
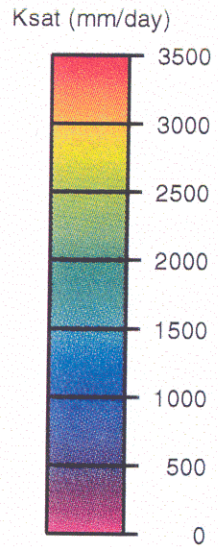
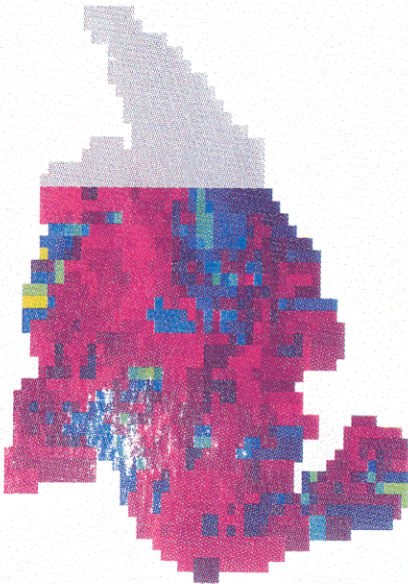
a) Total soil moisture storage capacity**b) Saturated hydraulic conductivity**

Figure 4.4 STATSGO derived soil parameters.

Initial estimates for the remaining five parameters as well as K_s and $W_{c,tot}$ for the Canadian region were taken from Nijssen et al. (1997). All seven soil parameters were then manually adjusted in areal blocks corresponding to the nine subbasins draining at each of the naturalized flow locations. Figure 4.5 shows the location of the nine subbasins and Table 4.3 describes relevant attributes.

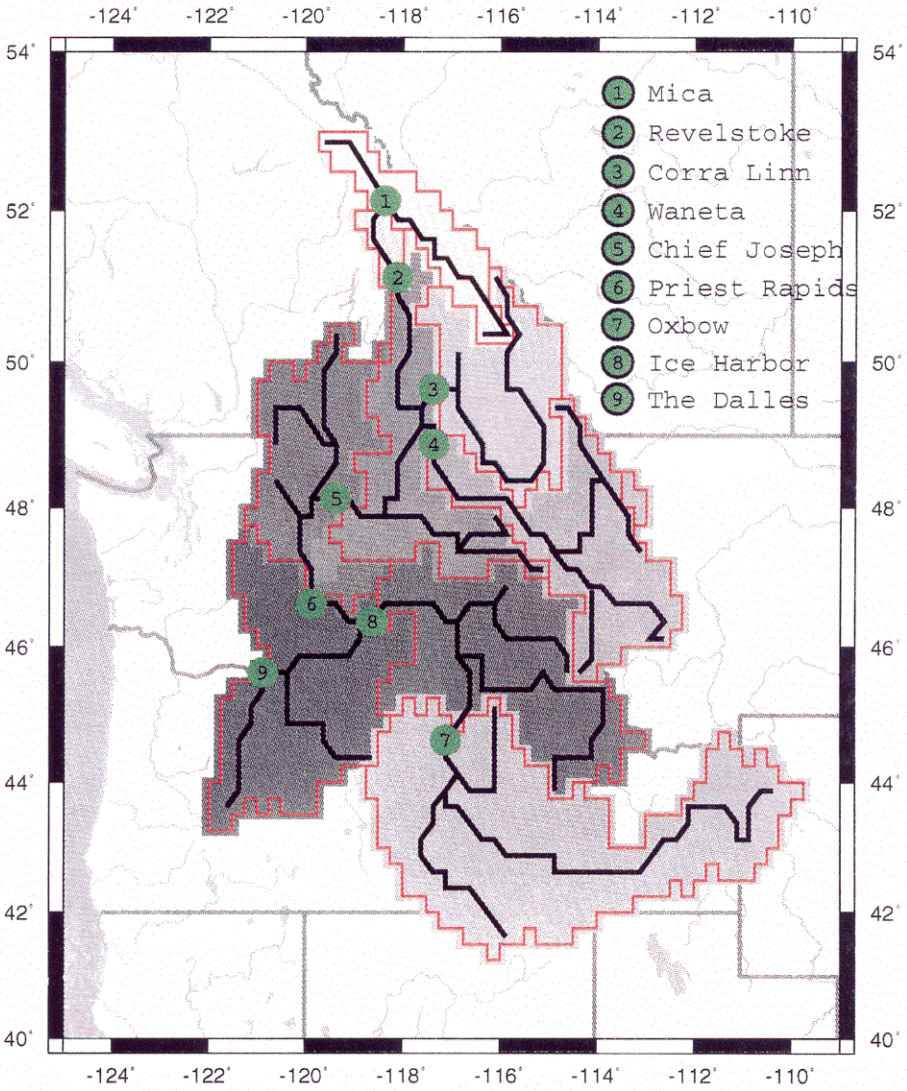


Figure 4.5 Subbasins contributing to nine naturalized flow locations.

Table 4.3 Subbasin river mile and drainage areas.

Subbasin	River	River Mile (upstream from mouth)	Drainage Area (mi ²)
Mica	Columbia	1018.1	8,290
Revelstoke	Columbia	934	10,200
Corra Linn	Kootenai	16.1	17,700
Waneta	Pend-Oreille	0.5	25,800
Chief Joseph	Columbia	545.1	75,400
Priest Rapids	Columbia	397.1	95,500
Oxbow	Snake	273	72,800
Ice Harbor	Snake	9.7	108,500
The Dalles	Columbia	191.5	237,000

Within each subbasin, adjustments were made uniformly for all grid cells and only one parameter per model run was adjusted. Heavily adjusted parameters included b_i , $W_{c,tot}$, W_s , $W_{2/1}$ and K_s (See Table 4.4). Among these parameters, $W_{c,tot}$, W_s and $W_{2/1}$ were adjusted the most. These parameters were found by Nijssen et al. (1997) to be among the most sensitive. The calibration was considered final when computed long-term mean seasonal and annual bias was minimized. Table 4.4 gives the range of soil parameters

used. Parameters which were subject to the most manual calibration are marked with an asterisk.

Table 4.4 Range of calibrated soil parameters. The symbol “*” indicates that the parameter was heavily adjusted.

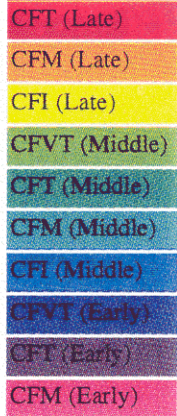
Parameter name	Symbol	Units	Range
Infiltration Parameter	bi*		0.1 - 0.25
Total soil moisture	Wc,tot*	mm	250 - 1500
Fraction of maximum baseflow	Ds		0.035 - 0.0475
Maximum baseflow	Dm	mm/day	5 - 11
Fraction of maximum baseflow at which baseflow computation becomes non-linear	Ws**		0.7 - 0.95
Ratio of soil moisture in bottom layer to top layer	W _{2/1} **		1 - 2
Saturated hydraulic conductivity	Ks**	mm/day	25 - 350

4.2.3 Vegetation parameters

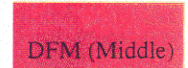
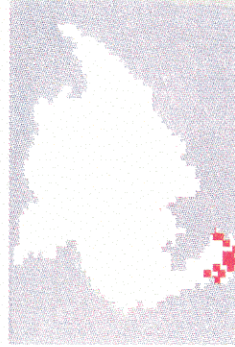
The vegetation parameters required by VIC-2L include maximum one-sided Leaf Area Index (LAI), minimum stomatal resistance, architectural resistance, roughness, length, zero plane displacement and root zone depth. The grid-cell value for each of these parameters was a function of the dominant vegetation cover type and/or structural stage within the grid cell, which were defined spatially at the model resolution for the current

and historical scenarios by the CVM and HVM, respectively. Figures 4.6 and 4.7 show the CVM and HVM.

a) Coniferous



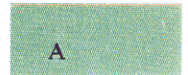
b) Deciduous



c) Rangeland



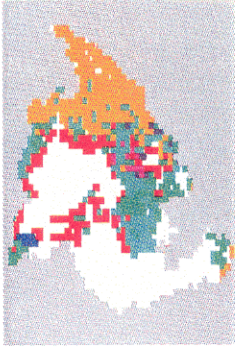
d) Agriculture



CFM = Coniferous forest, moderately drought tolerant	SM = Shrub, moderately drought tolerant
CFT = Coniferous forest, highly drought tolerant	ST = Shrub, highly drought tolerant
CFVT = Coniferous forest, very drought tolerant	G/F = Grasses/Forbs
CFI = Coniferous forest, drought intolerant	A = Agriculture
DFM = Deciduous forest, moderately drought tolerant	

Figure 4.6 Current vegetation map (CVM)

a) Coniferous



b) Deciduous



c) Rangeland



d) Agriculture



CFM = Coniferous forest, moderately drought tolerant	SM = Shrub, moderately drought tolerant
CFT = Coniferous forest, highly drought tolerant	ST = Shrub, highly drought tolerant
CFVT = Coniferous forest, very drought tolerant	G/F = Grasses/Forbs
CFI = Coniferous forest, drought intolerant	A = Agriculture
DFM = Deciduous forest, moderately drought tolerant	

Figure 4.7 Historical vegetation map (HVM)

4.2.3.1 Current and historical cover class maps

The vegetation cover class maps, CVM and HVM, depict the dominant cover type and structural stage within each model grid cell by a single integer corresponding with a vegetation class. The maps of cover type and structural stage ultimately used to produce the vegetation class maps in this study were derived from various existing maps as well as multivariate analysis to extrapolate structural stage data which were unavailable for the Canadian region. For the U.S., dominant cover classes were defined at quarter-degree resolution in the following manner:

- 1) combining grid-based maps of current cover type (CCT) and current structural stage (CSS) produced by Interior Columbia Basin Ecosystems Management Project (ICBEMP) and refined by Peter Thornton (University of Montana, Department of Forest Resources) at 2-km resolution to create a map of current vegetation class at 2-km resolution,
- 2) combining grid-based maps of historical cover types (HCT) and historical structural (HSS) produced by ICBEMP and refined by Thornton at 2-km resolution to create a map of historical vegetation class at 2-km resolution,
- 3) selecting the dominant vegetation class for quarter-degree blocks from the 2-km current and historical vegetation class maps and

- 4) resampling the dominant class maps to quarter-degree resolution.

ICBEMP data do not exist for the Canadian portion of the basin. Therefore, a different method was followed to prepare vegetation class maps for the region in Canada and is described later in this section.

The CCT data source referred to in step 1 represents existing vegetation types at 2-km resolution categorized by broad vegetation communities. Hardy et al. (1996) produced these data by reclassifying Advanced Very High Resolution Radar (AVHRR) Land Cover Classes (LCC) for North America (Loveland et al., 1991) into 48 aggregated cover types which better represent the vegetation communities of the CRB at coarse scale. Their method for producing the CCT was based on workshops with regional ecologists and model output from Columbia River Basin Successional Model (CRBSUM) (Keane et al., 1996). The forest and range cover types included in the CCT are mostly defined by the Society of American Foresters (Eyre, 1980) and Society of Range Management (Shiflet, 1994).

The CSS data source referred to in step 1 was developed by Hardy et al. (1996) using a discriminant analysis of the midscale structural stage data with topographical, climatic and vegetational indices held as independent variables. The midscale structural stage layer was developed as a part of the midscale subsample data (Hessburg and Smith, 1996) project, which mapped potential vegetation, cover types and structural stage from

1950 and 1990 aerial photography for watersheds in the CRB (covering approximately 3% of the CRB interior area). Topographical layers included elevation, aspect and slope, each derived from a 500-m DEM. Climate variables included annual precipitation, maximum and minimum temperature, dew point and solar radiation. Vegetation indices were derived from NDVI data for January, March, May, August and September, 1991. Independent discriminant functions were used for forest, woodland and range structural stages. The functions were applied over the rest of the basin (portion not covered in the midscale subsample data) with constraints imposed by the CRBSUM successional pathways.

Losensky et al. (1994) prepared the HCT map referred to in step 2, which broadly classifies historical cover types with an approximate target year of 1900 at 1:1,000,000 map scale. The data therein are a compilation of archived vegetation maps for the states of Idaho, Montana, Washington and Oregon with incongruous map scales and historical records published between 1900 and the late 1930's. Losensky et al. (1994) back-dated all information gathered after 1900 to the target year. In Western Montana, Northern Idaho and Northeast Washington, county-level field inventories prepared between 1932 and 1937 were used. Forest Service lands, which were relatively undisturbed at the time of the surveys, provided the basis for performing age structure analysis for the various cover types. The data from this analysis were then extended to the rest of the region, including privately owned lands. In Idaho, inventories were split between cut and uncut land, allowing for separate treatment of harvested lands. Harvested trees were assumed to

be mature or overmature in 1900. Burned areas were distributed between the various age classes based on the percentage of the cover type in a given age class. This method was used to represent the real nature of fires, in which trees of all ages are susceptible to burning. Available surveys were less complete in eastern Oregon and the rest of Washington. For these areas, the same methods as above were used when possible. Otherwise, trees were assumed to be equally distributed in 10-year increments for all age classes (Losensky et al., 1994). The authors noted that there was likely underestimation of mature and overmature age classes resulting from crude treatment of cutover forests. Furthermore, early harvest to support mining in some parts of Montana was likely misrepresented.

The HSS map (Hardy et al., 1996) referred to in step 2 was produced by a stochastic model nested inside the CRBSUM. Stochastic predictions of historical structural stage were based on summaries of percent occurrence of each structural stage by cover type reported by Losensky (1994). Within both the CSS and HSS maps, a total of 27 structural stage categories were used.

Thornton aggregated the cover type categories contained within the ICBEMP CCT and HCT data layers from 48 to 16 to produce new maps of current and historical cover type for the CRB at 2-km resolution. Table 4.5 lists these 16 cover types and their abbreviations.

Table 4.5 Description of VIC-2L cover types.

Value	Description	Abbreviation
1	Conifer, low drought tolerance	CFI
2	Conifer, moderate drought tolerance	CFM
3	Conifer, high drought tolerance	CFT
4	Conifer, very high drought tolerance	CFVT
5	Cottonwood/willow	DFI
6	Aspen	DFM
7	Oregon white oak	DFT
8	Herbaceous wetland/shrub	SI
9	Mountain shrub	SM
10	Sage shrub	ST
11	Grassland/forbs	G/F
12	Herbaceous wetland	W
13	Alpine tundra	T
14	Agriculture	A
15	Barren	N/A
16	Water	N/A

The resulting cover types will be referred to as “VIC-2L cover types” throughout this thesis. The method of aggregation used by Thornton was based on lifeform and drought tolerance. Drought tolerance was used to classify vegetation on the basis that many of the plant types in the CRB (especially in the northern region) are water-limited, rather than nutrient or light limited, and most adaptations are stimulated by water-stress (conversations with Peter Thornton, 1997). The aggregated cover type categories defined by Thornton consist of four levels of drought tolerance; intolerant (I), moderately tolerant (M), tolerant (T) and very tolerant (VT).

Thornton aggregated the number of structural stage categories used in the ICBEMP CSS and HSS maps from 27 to 4: early, middle, late and shrub. The early stage is analogous to stand initiation, where stem density is low, growth is not limited by space, mortality is negligible. Several (7) CSS/HSS structural stage categories were aggregated to form the middle stage, which represents light and nutrient limited growth with moderately high stem density. The late stage represents old-growth forest. A single structural stage (shrub) was used for all non-forest lifeforms (e.g., shrub, agriculture, barren and water). Thornton applied the aggregated structural stage categories, referred to in this thesis as “VIC-2L structural stages”, to produce new maps of current and historical structural stage at 2-km resolution.

Steps 1 and 2 proceeded by combining these refined maps of current and historical cover type and structural stage in Arc/Info to create maps of current and historical scenario vegetation class at 2-km resolution for the U.S. portion of the basin. Table 4.6

lists the various cover type and structural stage categories and vegetation classes associated with each combination. In step 3, the dominant vegetation class within quarter degree blocks was selected using the BLOCKMAJORITY command in Arc/Info and finally, in step 4, the dominant vegetation maps at 2-km resolution were resampled to quarter degree resolution using the RESAMPLE command in Arc/Info.

Because the ICBEMP cover type and structural stage data layers described above were unavailable for the Canadian portion of the basin, dominant cover classes were defined for the current and historical scenarios at quarter degree resolution for Canada with the following approach:

- 1) Reclassifying grid-based LCC maps of cover type for North America produced by Loveland et al. (1991) and regrouped into Simple Biosphere (SiB) cover types (Sellers et al., 1986) at 1-km resolution into VIC-2L cover types at 1-km resolution.
- 2) Resampling the CSS map for the U.S. produced by ICBEMP and refined by Thornton to 1-km resolution and extrapolating the data to Canada to produce a map of current scenario structural stage at 1-km resolution.
- 3) Applying a rule-based method for backdating the SiB cover types to the historical target date of 1900 to create a map of historical scenario cover type

at 1-km resolution.

- 4) Applying a rule-based method for defining the structural stage at 1-km resolution.
- 5) Combining the respective maps of VIC-2L cover type and structural stage produced in steps 1) through 4) into maps of VIC-2L vegetation class and aggregating to quarter degree resolution.

In step 1, the LCC map for North America, which was regrouped into Simple Biosphere (SiB) cover types (Sellers et al., 1986) at 1-km resolution, was used to define cover types for Canada. SiB is an energy balance SVATS with similar parameterizations for vegetation as those used by VIC-2L. Table 4.6 lists the SiB cover types which were present in the CRB and their abbreviations.

Table 4.6 SiB cover types and remap table used for reclassification.

SiB Code	Description	Remapped to VIC-2L cover type	VIC-2L cover type abbreviation
3	Deciduous and evergreen	3	CFT
4	Evergreen needleleaf	2	CFM
10	Groundcover with dwarf trees and shrubs	14	A

In order to have spatial consistency with the LCC map, Thornton's map of current cover types (CCT) was resampled to 1-km resolution. The next task in step 1 was to reclassify the SiB cover types to the 16 VIC-2L cover types defined by Thornton, which were extracted from the ICBEMP CCT map. This was done by analyzing a histogram of VIC-2L cover types verses SiB cover types for the U.S. Figure 4.8 shows the histogram used for this analysis. Although there was a significant degree of scatter between the two classification schemes, a majority cover type could be found for each SiB class and was ultimately used in the reclassification. Table 4.6 shows the reclass map used. The predominant SiB type in Canada (evergreen needleleaf trees) was reclassified to coniferous forest, moderate drought tolerance (CFM) and the second most frequent, deciduous and evergreen, was reclassified to coniferous forest, drought tolerant (CFT). Histograms of the Canadian vegetation cover types before and after reclassification are shown in Figure 4.9 and 4.10, respectively.

Percent coverage by VIC-2L cover type in U.S.

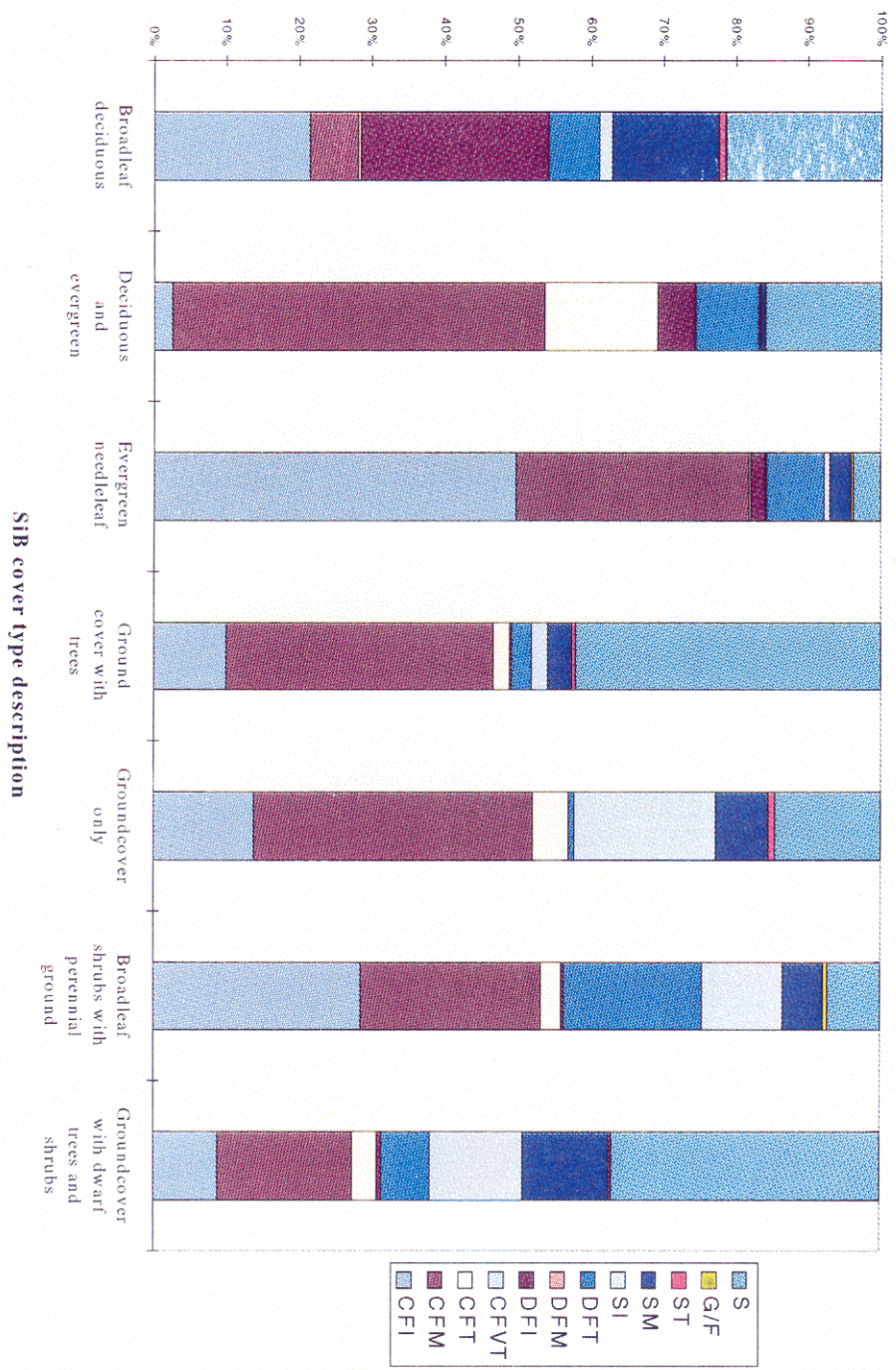


Figure 4.8 Histogram of VIC-2L cover types verses SIB cover types in the U.S. portion of the CRB.

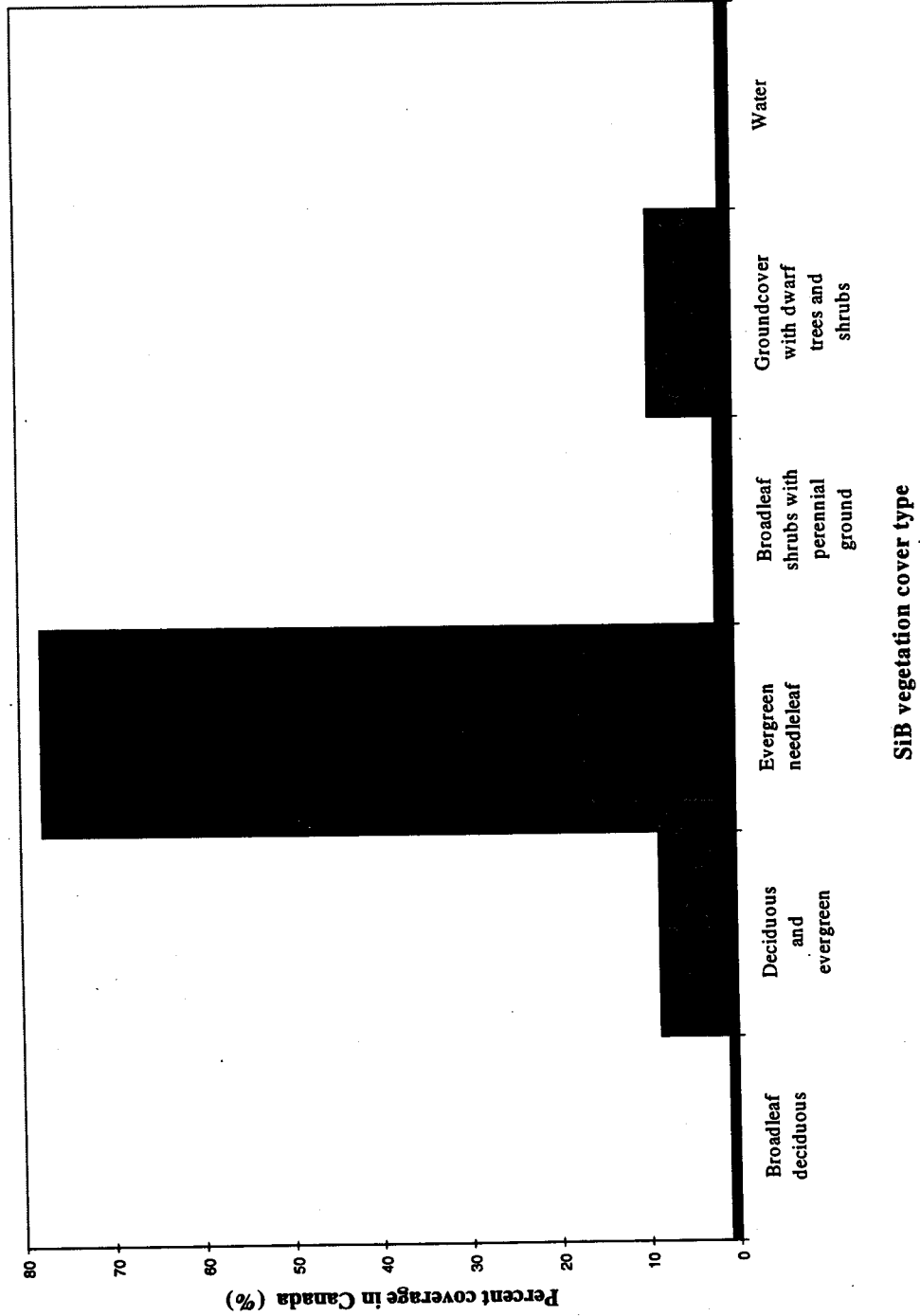


Figure 4.9 Histogram of SiB cover types in Canada (before reclassifying).

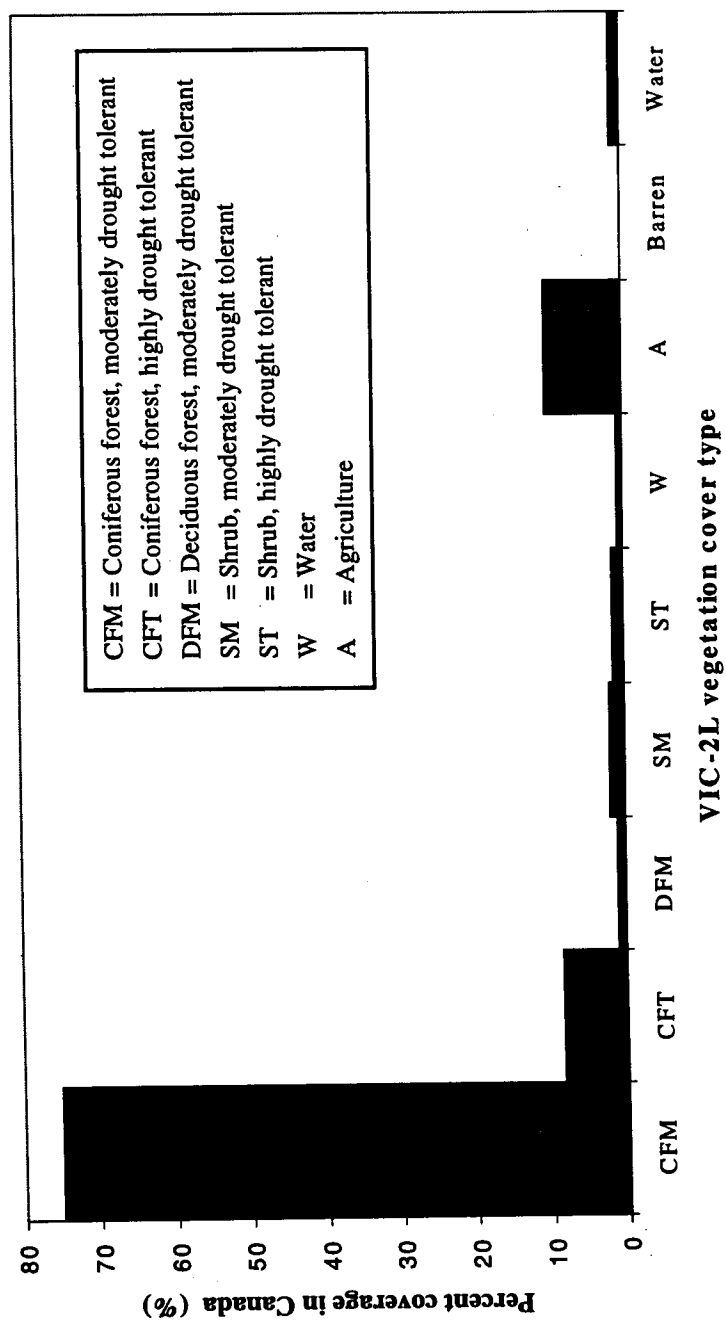


Figure 4.10 Histogram of VIC-2L cover types in Canada (after reclassification).

Step 2 was accomplished using monthly mean Normalized Difference Vegetation Index (NDVI) data for June, 1992 derived by Loveland (1991) from AVHRR data for North America. The basis of this method was that spatial differences in structural stage associated with a cover type should be related to spatial patterns in NDVI. This analysis was only performed for conifers, since deciduous trees are not dominant at the 1-km scale in Canada and age structure for non-forest lifeforms was considered unimportant relative to forest age. The method involved finding the mean and standard deviation of NDVI for all combinations of conifer types (coniferous forest, moderate drought tolerance (CFM) and coniferous forest, drought tolerant (CFT)) and structural stage in the U.S. Figure 4.11 shows histograms of NDVI for each of these combinations. The means were used to extrapolate current scenario structural stage to pixels in Canada covered by conifers, given NDVI. Table 4.7 shows the NDVI means and standard deviations for each coniferous type and structural stage.

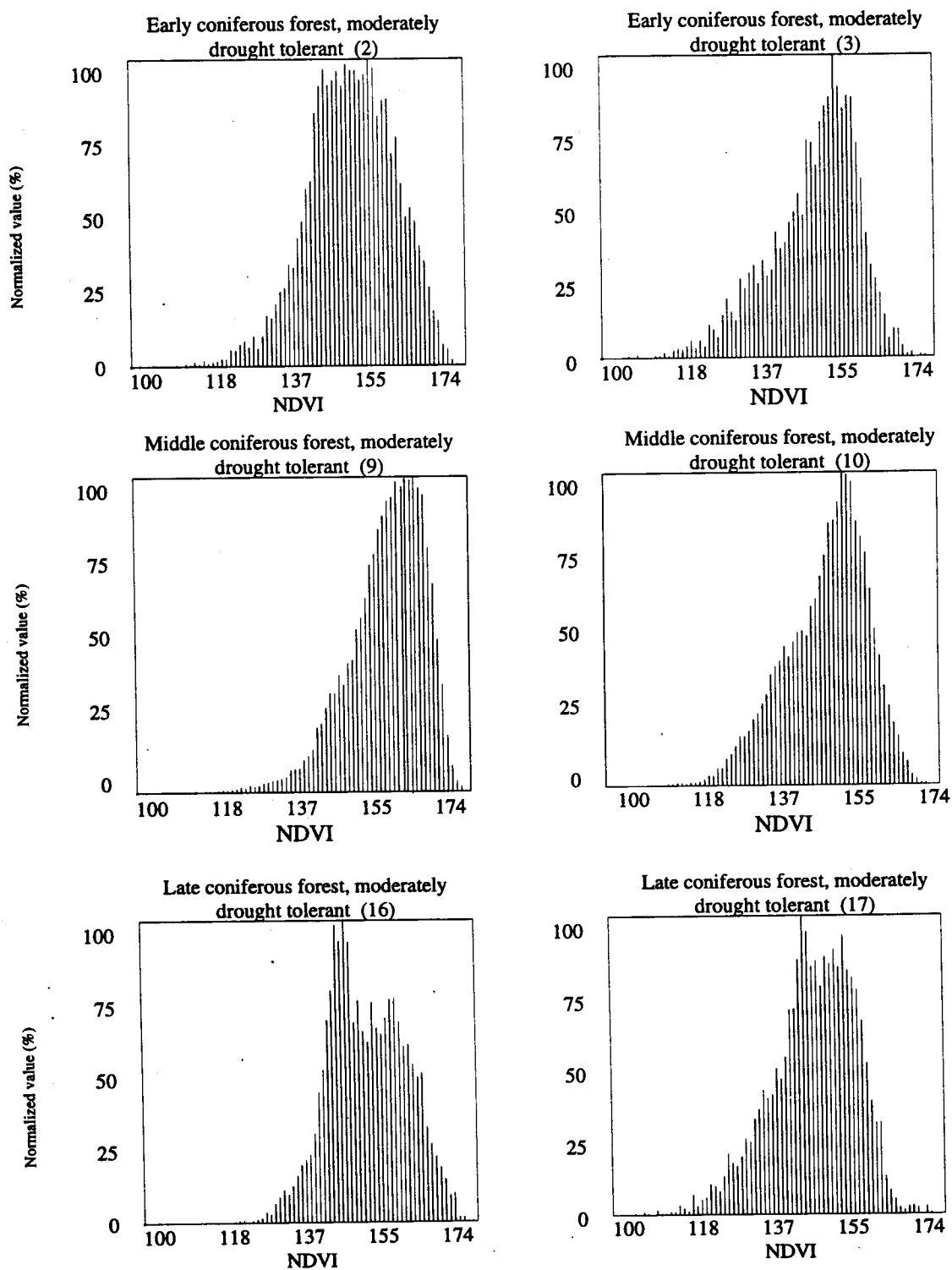


Figure 4.11 Histograms of NDVI for combinations of coniferous cover types and structural stage.

Table 4.7 Means and standard deviations for NDVI coupled with various combinations of coniferous forest and structural stage.

	Early	Middle	Late
CFI			
Mean	161.2	163.1	163.9
Standard Deviation	4.8	9.6	3.9
CFM			
Mean	148.5	154.9	149.3
Standard Deviation	12.3	12.8	1.8
CFT			
Mean	146.4	148.5	144.8
Standard Deviation	14.9	13.3	10.5
CFVT			
Mean	127.4	129.9	144.8
Standard Deviation	10.9	12.7	10.5

The map of current VIC-2L cover types derived above was backdated in step 3 to the historical scenario using two rules: a) forest cover types in the current scenario remained forest cover types in the historical scenario and b) agricultural pixels in the current scenario were set to shrubs with moderate drought tolerance (SM) in the historical scenario. Assignment of structural stages in Canada for the historical scenario (step 4) followed the rule that pixels covered by conifers with elevation lower than 1,000 m were assigned to the middle structural stage, while those with elevation equal to or exceeding 1,000 m were assigned to the late structural stage. This threshold value was applied to

represent the higher probability of forest fire at lower elevations (Heyerdahl et al., 1995).

In step 5, the current and historical maps of VIC-2L cover type and structural stage produced in the previous steps were combined and aggregated to quarter degree resolution in the same manner described for the U.S. This step created the final current and historical scenario VIC-2L vegetation class maps for the Canadian portion of the basin.

The resulting current and historical scenario maps for vegetation cover class at quarter-degree resolution for Canada were merged with corresponding vegetation cover class maps for the U.S. in Arc/Info using the MOSAIC command. This step produced continuous, quarter-degree resolution maps of current and historical VIC-2L vegetation class for the entire basin, referred to as CVM and HVM. These maps were used in combination with the look-up table to assign vegetation parameters to the grid cells. The final CVM and HVM maps are shown in Figures 4.6 and 4.7.

4.2.3.2 Parameter assignment

While the current and historical vegetation maps are much different with respect to frequency and distribution of classes, the same look-up table was used to assign parameters to the various classes for both scenarios. This method was consistent with the primary goal of the study, which was to evaluate the hydrologic effect of changing vegetation, rather than model sensitivity to parameter estimation for individual classes. A

second line of investigation, which addressed sensitivity to the rooting depth parameter with respect to structural stage, is discussed in Chapter 5.

The look-up table was used to assign maximum one-sided, or projected, leaf area index (LAI), maximum vegetation height, minimum stomatal resistance, architectural resistance and a root distribution parameter, f_2 , to the various modeling classes for the current and historical scenarios. Maximum projected LAI was prescribed following Thornton (1997). Thornton derived values for maximum projected LAI by first processing NDVI from the AVHRR data set. He used maximum values of NDVI from the 1990 bi-weekly composited AVHRR data in order to obtain highest values for all cover types. He next separated the NDVI data into three broad vegetation groups, evergreen/coniferous, deciduous/broadleafed and grass/arid/cropland, using the original ICBEMP current scenario cover type data layer at 2-km resolution. Separate literature derived equations were used to compute LAI for each broad vegetation group as a function of the filtered maximum NDVI values for the various ICBEMP vegetation cover types.

The minimum and maximum values of projected LAI obtained by this method were 1.0 and 13.0 for evergreen, 1.0 and 8.0 for deciduous and 0.5 and 3.0 for the grass crops. Thornton made summaries of average LAI by his modified cover type and structural stage data layers, which were aggregated from the ICBEMP CCT and CSS data sources as described in Section (4.2.3.1). For each combination of cover type and structural stage, he compared his NDVI-derived LAI value with literature values (Waring and Franklin,

1979). Because his values were higher than the literature values, he applied correction coefficients which were derived as the ratio of the expected (literature) value over his average NDVI-LAI value. These corrected values for LAI were directly applied in this study for maximum one-sided LAI and are shown for all combinations of cover type and structural stage (VIC-2L vegetation cover class) in Table 4.6.

LAI seasonality was applied as a monthly fraction of the maximum value to agriculture and deciduous cover types, while conifers were assumed to have constant LAI throughout the year. LAI seasonality for U.S. agricultural crops was reported by Xue et al. (1996). Seasonality of forest species was evaluated at 1-km spatial resolution and aggregated to quarter degree from monthly composited NDVI values for 1992 from the AVHRR North American data set. The monthly fractions were assigned as the monthly composited NDVI divided by the monthly composited NDVI for June.

Minimum stomatal resistance values were derived as the inverse of maximum stomatal resistance obtained from Thornton (1997). Thornton derived values for maximum stomatal resistance from various literature sources. He obtained values for coniferous species from Kelliher et al. (1995), who report an average maximum stomatal resistance of 0.0057 m/s with a sample standard deviation of 0.0024 m/s based on field data from 26 conifer species. Other published values were in agreement with those provided by Kelliher et al. for coniferous species (Hinckley et al., 1978; Korner et al., 1979). These literature sources also indicated that drought tolerant coniferous species have lower maximum stomatal resistance than species which are less drought tolerant.

Thus, Thornton distributed the maximum coniferous stomatal resistance between the four drought tolerance classes, giving the two middle drought tolerance classes the average value reported by Kelliher et al. (1995), subtracting one standard deviation from the average for the highest drought tolerance class and adding one standard deviation to the average for the lowest drought tolerance class. Deciduous and shrub cover types received slightly higher values for maximum stomatal resistance than conifers, with similar variation among the drought tolerance classes. Thornton used a value of .008 m/s for grasses and the highest value (0.01 m/s) for herbaceous wetland and agricultural classes to account for adaptation to low water stress environment. No consideration was made of structural stage for any of the cover types.

Maximum vegetation height for the 16 VIC-2L cover types was assessed as the maximum height of a single key species contained within each broad VIC-2L cover type category. For instance, the VIC-2L cover type coniferous forest, moderate drought tolerance (CFM) contains approximately 10 original ICBEMP coniferous species. Maximum height was assessed for Pacific silver fir, which is among the 10 original species, and assumed to equal the maximum height for the VIC-2L cover type category CFM. The selection of key species within each VIC-2L cover type category and assessment of maximum height for that species was based on Burns et al. (1990) and conversations with Professor Tom Hinckley (College of Forest Resources, University of Washington). The late structural stage category was assigned the maximum height for each VIC-2L cover type, since it represents the oldest age class. Early and middle

structural stages were assigned 25% and 50% of the maximum height for a given VIC-2L cover type, respectively, as suggested by Hinckley (1997). This method was highly subjective, since categories for type and structural stage are broad and were applied to large pixels (quarter-degree resolution) which are assumed to have homogeneous vegetation. Roughness and displacement lengths were calculated as a function of vegetation height following Calder (1993).

The vegetation parameter f_2 assigns a percentage of the roots to the bottom model soil layer. This parameter was estimated as 50% for all forest cover classes with early structural stage, 20% for shrubs and 10% for agriculture following Nijssen et al. (1997). f_2 for forest types with middle and late structural stage was specified somewhat arbitrarily, since data and literature regarding the growth of roots with respect to structural stage are unavailable. The value used was 55%, chosen to represent the probability of roots extending deeper below the ground with succession between the early and middle structural stages. A sensitivity analysis of this parameter was performed and is described in Chapter 5.

Table 4.8 Look-up table used to assign parameters to VIC-2L vegetation classes.

cover	structural	Class	VIC-2L class	LAI _{max}	Height	Rs	Rarc
type	stage	(#)	abbreviation		(m)	(s/m)	(s/m)
1	1	1	CFI-early	12.0	10.0	125.0	40.0
2	1	2	CFM-early	6.0	8.75	166.6	40.0
3	1	3	CFT-early	4.0	7.5	166.6	40.0
4	1	4	CFVT-early	1.0	2.5	250.0	40.0
5	1	5	DFI-early	2.0	6.25	100.0	50.0
6	1	6	DFM-early	2.0	5.0	125.0	50.0
7	1	7	DFT-early	2.0	5.0	166.6	50.0
1	2	8	CFI-middle	14.0	20.0	125.0	40.0
2	2	9	CFM-middle	9.0	17.5	166.6	40.0
3	2	10	CFT-middle	6.0	15.0	166.6	40.0
4	2	11	CFVT-middle	2.3	5.0	250.0	40.0
5	2	12	DFI-middle	3.0	12.5	100.0	50.0
6	2	13	DFM-middle	3.0	10.0	125.0	50.0
7	2	14	DFT-middle	3.0	10.0	166.6	50.0
1	3	15	CFI-late	15.5	40.0	125.0	40.0
2	3	16	CFM-late	7.0	35.0	166.6	40.0
3	3	17	CFT-late	5.0	30.0	166.6	40.0

4	3	18	CFVT-late	2.0	10.0	250.0	40.0
5	3	19	DFI-late	3.5	25.0	100.0	50.0
6	3	20	DFM-late	3.5	20.0	125.0	50.0
7	3	21	DFT-late	3.5	20.0	166.6	50.0
8	4	22	SI-shrub	2.0	2.0	100.0	2.5
9	4	23	SM-shrub	1.5	2.0	125.0	2.5
10	4	24	ST-shrub	1.5	2.0	166.6	2.5
11	4	25	G/F-shrub	1.5	1.0	125.0	2.5
12	4	26	W-shrub	2.2	1.0	100.0	2.5
13	4	27	T-shrub	0.5	1.0	166.6	2.5
14	4	28	A-shrub	2.3	1.0	100.0	3.0
15	4	29	N/A	1.0	0.5	80.0	2.5
16	4	30	N/A	1.0	0.5	80.0	2.5

4.3 Calibration and test results

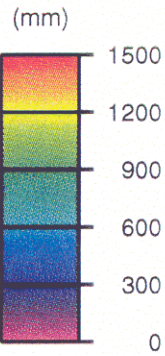
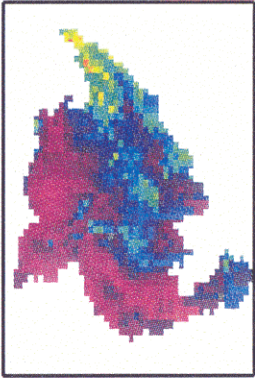
Section 4.3 discusses the model results for the calibration and test periods, October, 1983 - September, 1986 and October, 1986 - September, 1989, respectively. Maps of mean annual precipitation, runoff and evaporation show the long term water balance of VIC-2L inputs and outputs. Also presented are mean monthly hydrographs of current scenario simulated and naturalized flow, which graphically demonstrate the relative performance of the model in simulating peak timing and magnitude as well as long term annual volumes with respect to the mean monthly naturalized flows for the various subbasins. Relative bias and relative root mean square error were calculated for annual time steps and for 3-month seasons to provide a quantitative measure of performance.

4.4 Mean annual precipitation, runoff and evaporation

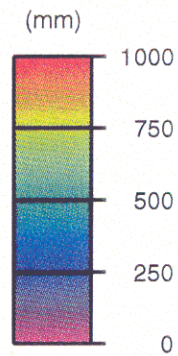
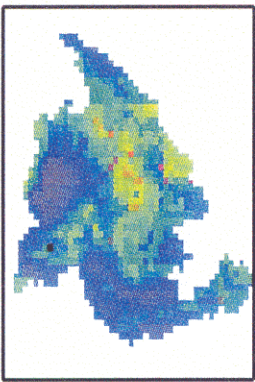
Figure 4.12 shows the mean annual precipitation and simulated runoff and evaporation for the current scenario calibration period simulation. The precipitation map is the long-term annual average of the daily gridded precipitation time series input to the VIC-2L. The evaporation and runoff maps are annually averaged VIC-2L daily output series, where daily runoff is the sum of direct runoff and baseflow. Since changes in soil moisture are negligible on an annual time scale, evaporation and runoff sum to equal the precipitation for each grid cell.

As noted in Section 2.1, precipitation within the modeled region is highest along the northern boundary in Canada and on the Western boundary above the Dalles, ranging from 1,000-2,500 mm. It is lowest in the semiarid southeastern region. The basin-wide mean annual precipitation ranges between 200 and 2500 mm. Mean annual evaporation for the simulation period ranged between 100 and 900 mm and was highest in the eastern portion of the basin coinciding with the region of highest temperatures. Simulated mean annual runoff varied between 50 and 1250 mm with highest values in the north and lowest in the southeast.

a) precipitation



b) evaporation



c) runoff

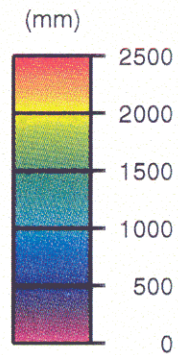
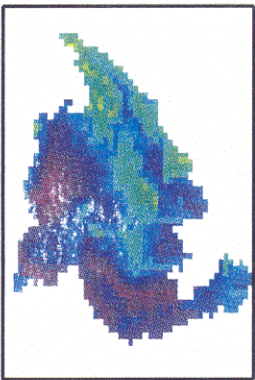


Figure 4.12 Mean annual water balance for the calibration period.

4.5 Relative bias

Relative bias in the simulated flows was calculated as:

$$\text{bias} = \frac{\bar{Q}_s - \bar{Q}_n}{\bar{Q}_n} \times 100\% \quad (19)$$

where, \bar{Q}_s and \bar{Q}_n are simulated and naturalized flows, respectively, averaged over monthly, seasonal and annual periods. Tables 4.9 and 4.10 show the relative bias for the calibration and test periods at all nine locations.

4.6 Relative root mean square error

Relative root mean square error (RRMSE) was calculated as:

$$\text{RRMSE} = \frac{\left[(1/n) \sum_{i=1}^n (Q_{s,i} - Q_{n,i})^2 \right]^{1/2}}{\bar{Q}_n} \quad (20)$$

where, n is the total number of months within the period of calculation. RRMSE was calculated seasonally and annually for the calibration and test periods. Tables 4.9 and 4.10 show the RRMSE values.

4.7 Monthly hydrographs

Figures 4.13 and 4.14 show the mean monthly hydrographs for the calibration and test periods for all nine subbasins. The hydrograph at Waneta was noted (Nijssen et al., 1997) as being typical for the Columbia basin, with a pronounced snowmelt peak in the spring and early summer causing streamflows to be roughly 5 times greater than in fall and winter months. The model closely reproduced the timing and magnitude of the naturalized hydrograph for this location.

The hydrograph for the calibration period at Corra Linn near the mouth of the Kóotenai shows poor timing of the peak flow, with the underprediction in May roughly equal to the overprediction in July. This error in timing propagates downstream to Chief Joseph and Priest Rapids. Nonetheless, the predicted annual volumes are within 3% of the observed at all 3 locations. The timing error is attributed to a delay in spring snowmelt simulated by the snow model. Figures 4.2 and 4.3 show that the simulated snow cover persists throughout the spring of 1994 in the U.S. region contributing to Corra Linn. This is contrary to the observed snow extent for the same region, which shows that only a few grid cells within Corra Linn have snow after the month of January. It should be kept in mind, however, when using the GOES data to evaluate the instantaneous snow extent that the monthly hydrographs represent mean monthly values averaged over three years of simulation (1983 - 1986), where the GOES data are instantaneous values taken during a

later period (1990-1995). Furthermore, the GOES data may underestimate snow areal coverage, due to the difficulty of detecting snow under trees with satellite imagery.

The hydrographs at Ice Harbor and Oxbow Dam on the Upper Snake River in the southeastern part of the basin show the poorest agreement in terms of timing and magnitude with naturalized flows of any of the nine subbasins. The hydrology of the upper portion of the subbasin is dominated by groundwater effects. According to Nijssen et al. (1997), this is suggested by the relatively damped seasonal cycle of the hydrograph at Ice Harbor near the mouth of the Upper Snake River with respect to seasonal precipitation. Nijssen et al. also noted that at coarse model resolution, the accuracy of the river routing network, where flow from each cell is discharged to only one neighboring cell and all cells are relegated to only one subbasin, may significantly contribute to simulation error, especially in drier regions. Furthermore, the Upper Snake region is the driest area within the basin, with a spatially averaged mean annual precipitation of approximately 500 mm (roughly one-fifth that of the wettest northern and western regions). Abdulla and Lettenmaier (1997) also noted that the VIC-2L tends to perform worse in dry regions than in wetter ones.

Predicted hydrographs for Mica and Revelstoke show fairly good agreement with naturalized flows during winter, spring and fall, but considerable underestimation of summer runoff. It is interesting to note that Nijssen et al. only slightly underestimated summertime flows at these locations with comparable precipitation input, and snow and soil parameters. Most of the vegetation parameters, including maximum LAI, minimum

stomatal resistance and architectural resistance used in both studies for the Canadian region (dominated by coniferous forest) are nearly identical to those used by Nijssen et al. as well. The difference may lie in the estimation of vegetation heights, which determine the aerodynamic resistance to evaporation. In this study, tree heights were assumed to be a function of structural stage, with 25, 50 and 100 percent of the maximum estimated height being assigned to the early, middle and late structural stages, respectively. For early conifers in Canada (with moderate drought tolerance), the height used in this study was 10 m, as opposed to 17 m used in the application by Nijssen et al. This difference in mean pixel vegetation height could result in approximately 20% lower aerodynamic resistance to evaporation, assuming a wind speed of 8 m/s at 300 m with a meteorological station height of 2 m.

Finally, the simulated hydrograph at the Dalles is in good agreement with the naturalized flows for the calibration period. The simulated timing of peak runoff is slightly late, presumably carrying over from the lag in spring snowmelt at Corra Linn. The timing error is worse for the test period. It can be expected that better calibration of the maximum and minimum melt factors, especially in the northeastern part of the basin, would result in better prediction of peak runoff timing. However, the prediction of annual runoff volumes for both the calibration and test periods are within 5% and show improvement over the one-degree application by Nijssen et al. Where annual average runoff volumes were underestimated in this study by 0.9 and 3.5% for the calibration and test periods, respectively, Nijssen et al. reported positive relative annual bias of 11.8% for

the period 1960 - 1988.

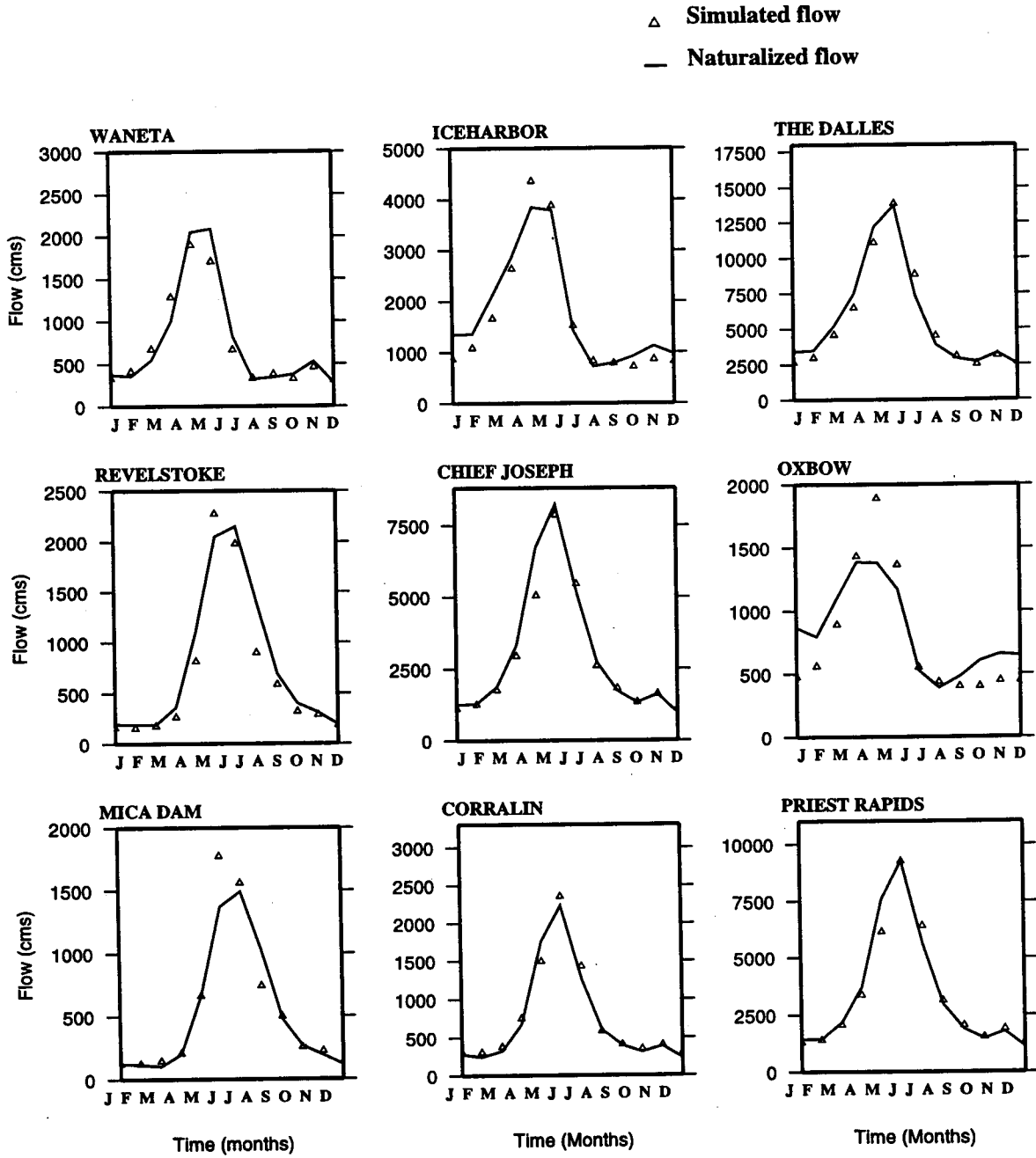


Figure 4.13 Simulated and naturalized mean monthly streamflow for calibration period October, 1983 - September, 1986.

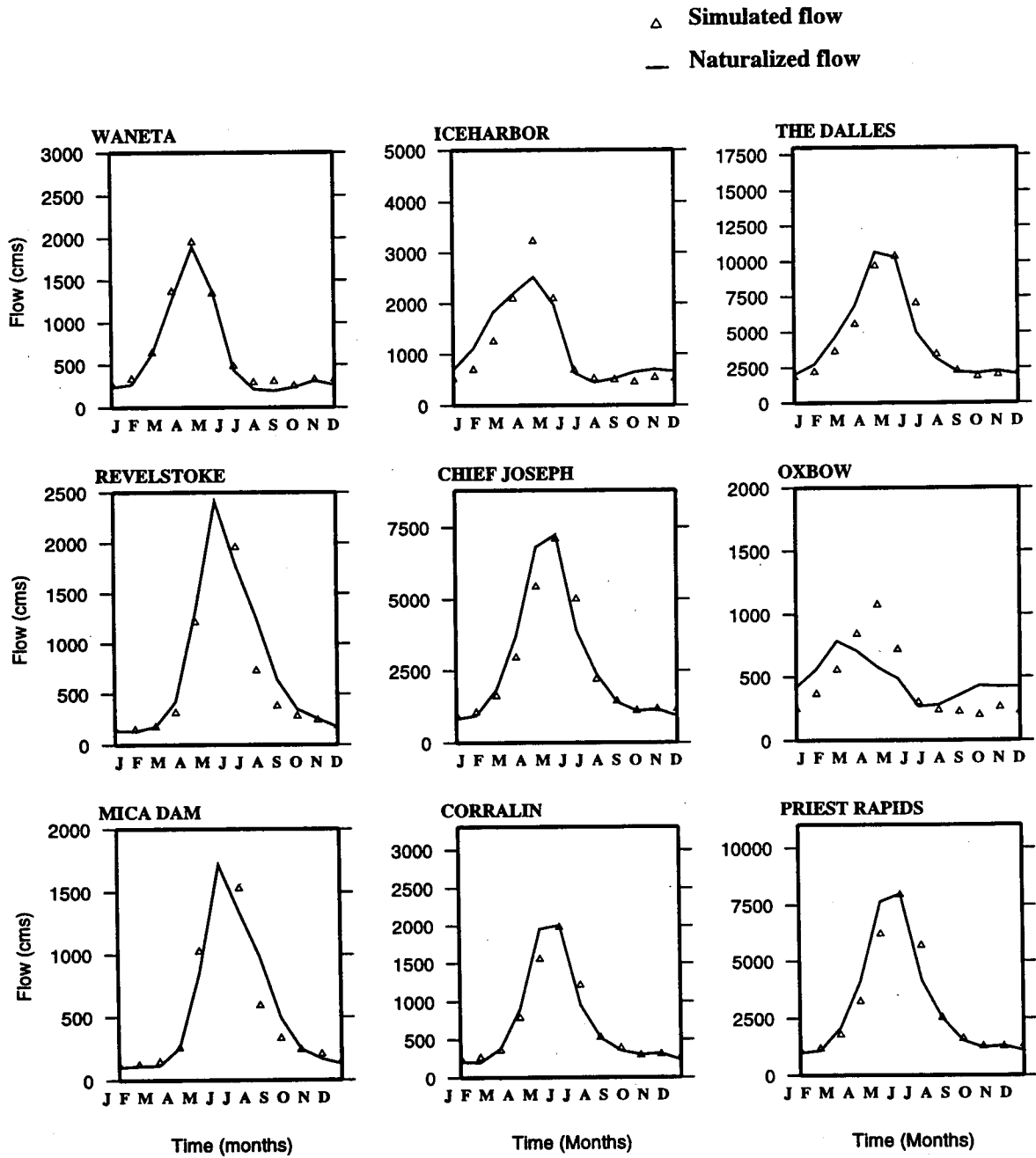


Figure 4.14 Mean monthly hydrographs for the test period October, 1986 - September, 1989.

Table 4.9 Relative bias and root mean square error for the calibration period.

		Calibration, 1983-1986				
Location	Statistic	<u>Annual</u>	<u>Fall</u>	<u>Winter</u>	<u>Spring</u>	<u>Summer</u>
Mica (1)	bias	4.8	7.2	13.4	18.1	-6.6
	RRMSE	0.12	0.29	0.19	0.23	0.08
Revelstoke (2)	bias	-12.6	-13.1	-14.4	-4.6	-18.8
	RRMSE	0.28	0.29	0.15	0.10	0.19
Corra Linn (3)	bias	4.2	12.4	16.8	-1.3	7.6
	RRMSE	0.15	0.14	0.20	0.11	0.13
Waneta (4)	bias	-3.5	-7.3	10.1	-4.7	-7.6
	RRMSE	0.07	0.11	0.12	0.18	0.13
Chief Joseph (5)	bias	-6.0	5.3	-5.6	-13.1	2.6
	RRMSE	0.11	0.09	0.12	0.16	0.06
Priest Rapids (6)	bias	-1.32	9.4	-5.2	-8.6	10.4
	RRMSE	0.05	0.11	0.12	0.13	0.13
Oxbow (7)	bias	-6.5	-32.3	-36.7	22.3	7.2
	RRMSE	0.14	0.33	0.37	0.23	0.11
Ice Harbor (8)	bias	3.0	-15.2	-23.0	17.2	13.6
	RRMSE	0.10	0.16	0.25	0.22	0.21
The Dalles (9)	bias	-1.0	-3.0	-14.1	-2.8	15.6
	RRMSE	0.04	0.03	0.16	0.10	0.17

Table 4.10 Relative bias and root mean square error for the test period.

		Test period, 1986-1989				
Location	Statistic	<u>Annual</u>	<u>Fall</u>	<u>Winter</u>	<u>Spring</u>	<u>Summer</u>
Mica (1)	bias	4.9	8.7	16.9	20.1	-12.7
	RRMSE	0.15	0.13	0.18	0.21	0.14
Revelstoke (2)	bias	-7.6	-9.5	5.3	-0.4	-16.9
	RRMSE	0.10	0.11	0.07	0.03	0.19
Corra Linn (3)	bias	-1.6	4.2	10.6	-11.4	16.11
	RRMSE	0.19	0.14	0.20	0.14	0.22
Waneta (4)	bias	7.9	12.7	10.7	2.8	27.1
	RRMSE	0.06	0.19	0.23	0.16	0.28
Chief Joseph (5)	bias	-3.0	9.3	0.7	-12.7	12.34
	RRMSE	0.07	0.12	0.14	0.14	0.15
Priest Rapids (6)	bias	-1.8	6.6	-3.5	-11.9	19.5
	RRMSE	0.13	0.11	0.15	0.14	0.22
Oxbow (7)	bias	0.46	-40.2	-20.3	54.4	-7.2
	RRMSE	1.45	0.47	0.32	0.70	0.12
Ice Harbor (8)	bias	-5.8	-19.6	-23.9	3.6	12.7
	RRMSE	0.70	0.26	0.36	0.15	0.15
The Dalles (9)	bias	-3.5	-6.0	-18.5	-7.9	23.4
	RRMSE	0.29	0.09	0.28	0.13	0.25

5. Current and historical scenario simulation results

In this chapter, the hydrologic results from the current and historical scenario streamflow predictions for the entire simulation period October, 1980 to September, 1995 are compared. Mean monthly hydrographs with a superimposed monthly relative percent difference trend-line provide the basis for the qualitative discussion of results. Maps of mean monthly baseflow and evaporation output directly by the VIC-2L for selected subbasins are presented to illustrate the spatial differences in water partition which affect the ultimate differences in streamflow. Relative percent differences between the mean monthly current and historical simulated flows for monthly, 3-month seasons and annual time steps are provided to quantify the results. The sensitivity analysis of the vegetation parameter which distributes the roots between the top and bottom soil compartments is also discussed.

5.1 Relative percent difference

Relative percent difference (RPD) was calculated as:

$$RPD = \frac{\bar{Q}_c - \bar{Q}_h}{\bar{Q}_c} \times 100\% \quad (21)$$

where, \bar{Q}_c and \bar{Q}_h are simulated mean monthly current and historical flows, respectively.

Table 5.1 reports the calculated values of seasonal and annual calculated values of RPD.

Table 5.1 Annual and seasonal RPD for all locations.

Simulation period October, 1980 - September, 1995					
Location	<u>Annual</u>	<u>Fall</u>	<u>Winter</u>	<u>Spring</u>	<u>Summer</u>
Mica (1)	6.6	0.8	2.8	4.4	8.5
Revelstoke (2)	6.5	8.2	1.5	4.4	9.3
Corra Linn (3)	6.0	0.7	1.8	5.4	10.8
Waneta (4)	-9.2	-13.9	-8.8	-7.3	-12.7
Chief Joseph (5)	0.9	-2.9	-3.4	0.22	5.4
Priest Rapids (6)	2.0	-2.5	-2.4	1.8	6.0
Oxbow (7)	-0.8	-4.9	-2.9	2.5	-3.7
Ice Harbor (8)	-0.3	-2.5	-3.1	1.1	0.1
The Dalles (9)	0.7	-4.5	-2.9	1.2	4.5

5.2 Mean monthly hydrographs and relative percent difference

Figure 5.1 shows mean monthly hydrographs for the current and historical scenarios for all nine subbasins with the dashed-crossed line representing monthly relative percent difference (RPD). The hydrographs at Mica, Revelstoke and Corra Linn show large mean annual increases in streamflow resulting from the changed vegetation cover classes and corresponding differences in vegetation parameters. Figures 4.6 and 4.7 show the spatial vegetation distribution for the current and historical scenarios, respectively. The current scenario vegetation for the pixels draining at Revelstoke, including those draining at Mica, contains mostly early coniferous forest, moderately drought tolerant (CFM-early) with a few scattered agricultural pixels. The historical scenario vegetation for these locations consists primarily of old growth coniferous forest, moderately drought tolerant (CFM-late) and moderately drought tolerant shrubs in place of the current scenario agriculture. Table 5.2 summarizes the major differences in vegetation parameters resulting between the current and historical scenarios for Revelstoke and Mica.

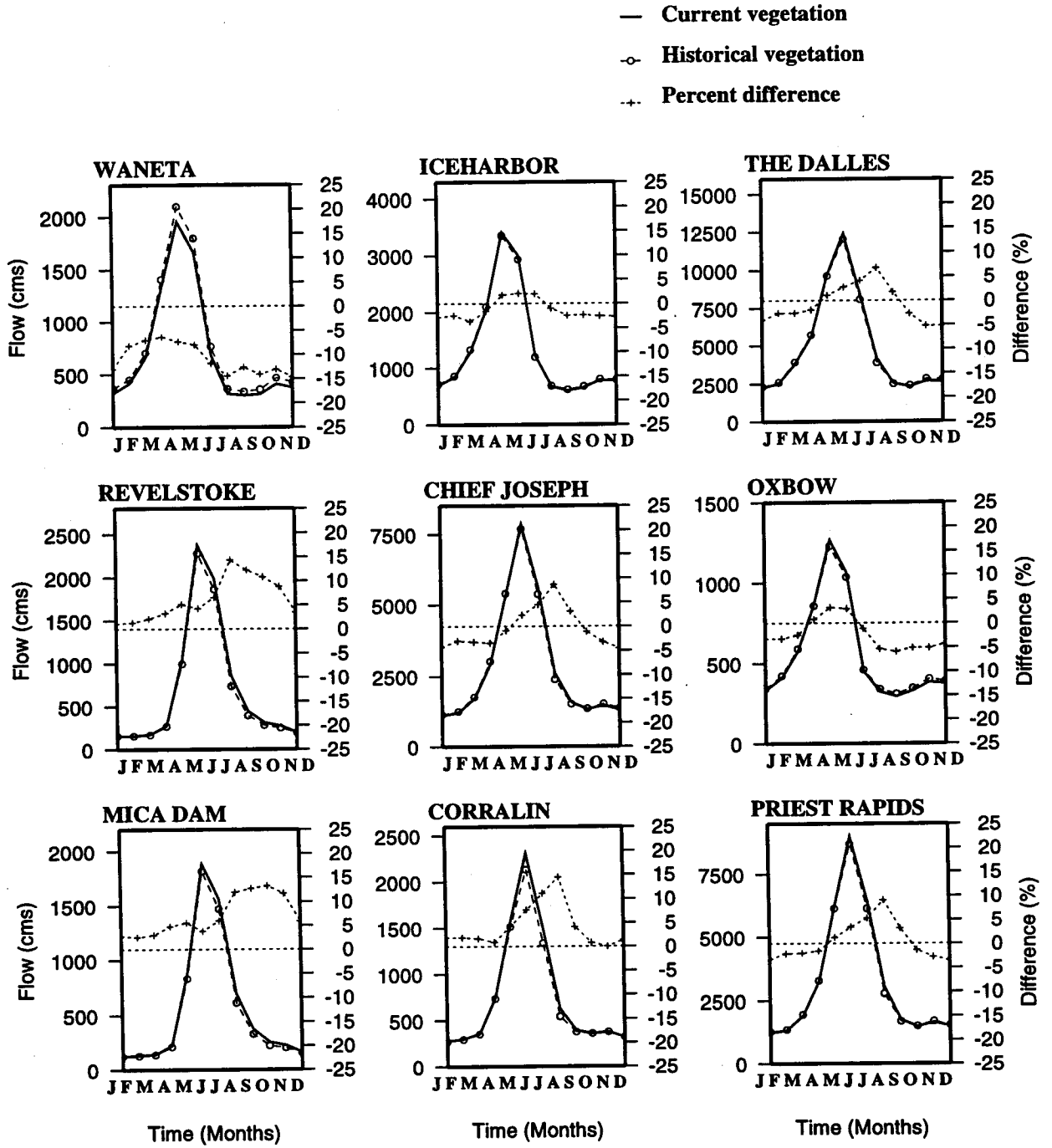


Figure 5.1 Mean monthly hydrographs for the current and historical vegetation scenarios and relative percent difference.

Table 5.2 Subbasin-wide dominant vegetation classes and parameter values for the current and historical scenarios at Revelstoke and Mica.

	Current scenario	Historical scenario
VIC-2L vegetation cover		
class	CFM-early	CFM-late
LAI _{max}	6.0	7.0
Height (m)	8.75	35.0
r_s (m/s)	166.6	166.6
r_{arc} (m/s)	40.0	40.0
f2 (%)	50	55

The current scenario hydrograph at Revelstoke is approximately 15 percent higher in late summer than in the historical scenario. This large difference is attributed to summer evaporation, which is enhanced in the historical scenario by the higher maximum LAI and deeper extension of roots into the bottom soil layer. Figure 5.2 shows the differences in late summer evaporation between the current and historical scenarios at Revelstoke and Mica, with differences expressed relative to the current scenario. Long-term mean historical evaporation for the month of August exceeds evaporation for the current scenario by roughly 15 percent on average and by 35 percent in the central part of the region. The current scenario hydrograph remains substantially higher throughout the fall

as the result of lower transpiration in the summer and higher baseflow in subsequent months. Figure 5.3 illustrates the simulated differences in baseflow for October. Monthly RPD approaches zero in December and remains below 5 percent during the winter, where positive values for RPD indicate that the current scenario predicted streamflow is higher than the historical scenario prediction. In spring, increased historical scenario evaporation and reduced baseflow account for a seasonal RPD of approximately 5 percent. Figure 5.4 shows mean evaporation for May at Revelstoke and Mica, with differences in evaporation ranging from 5 to 15 percent globally in both regions.

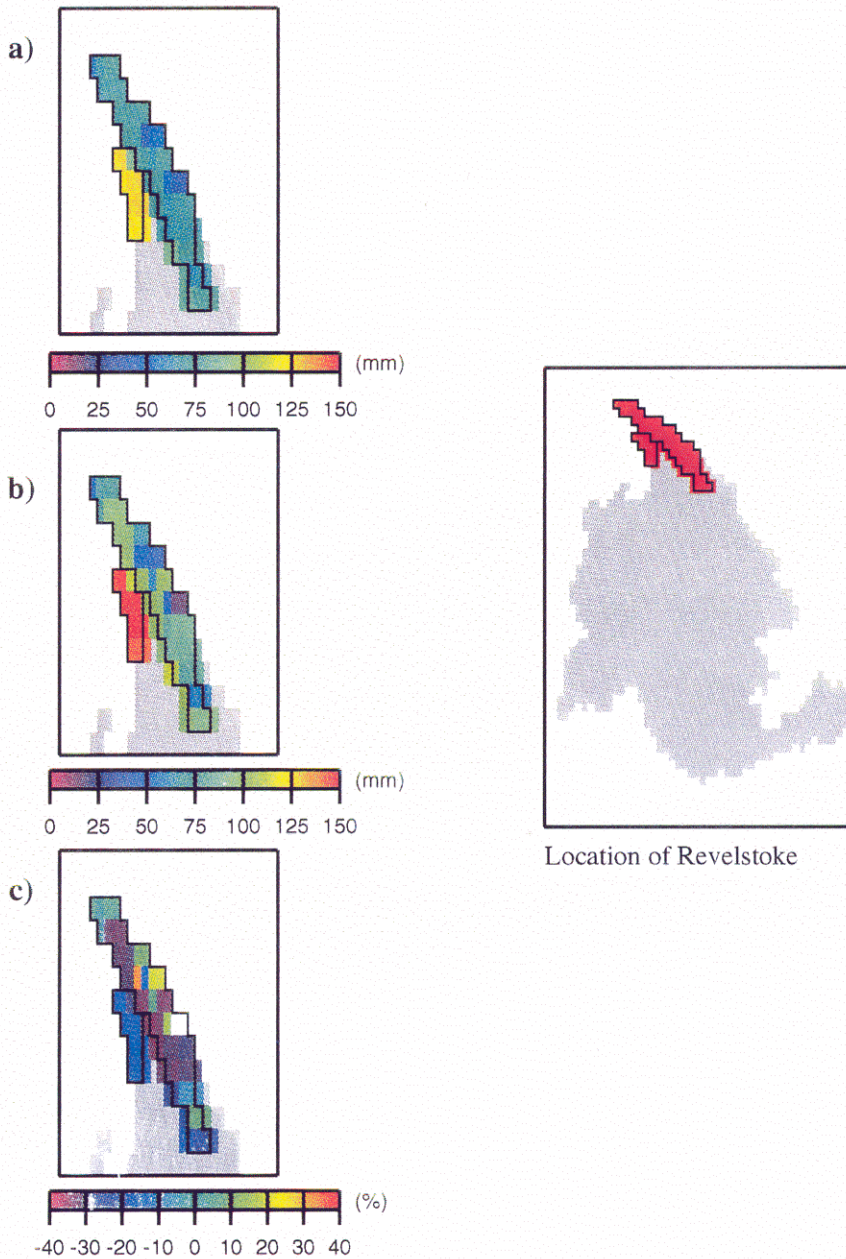


Figure 5.2 Simulated mean monthly a) current, b) historical and c) percent difference in evaporation for the month of August at Revelstoke.

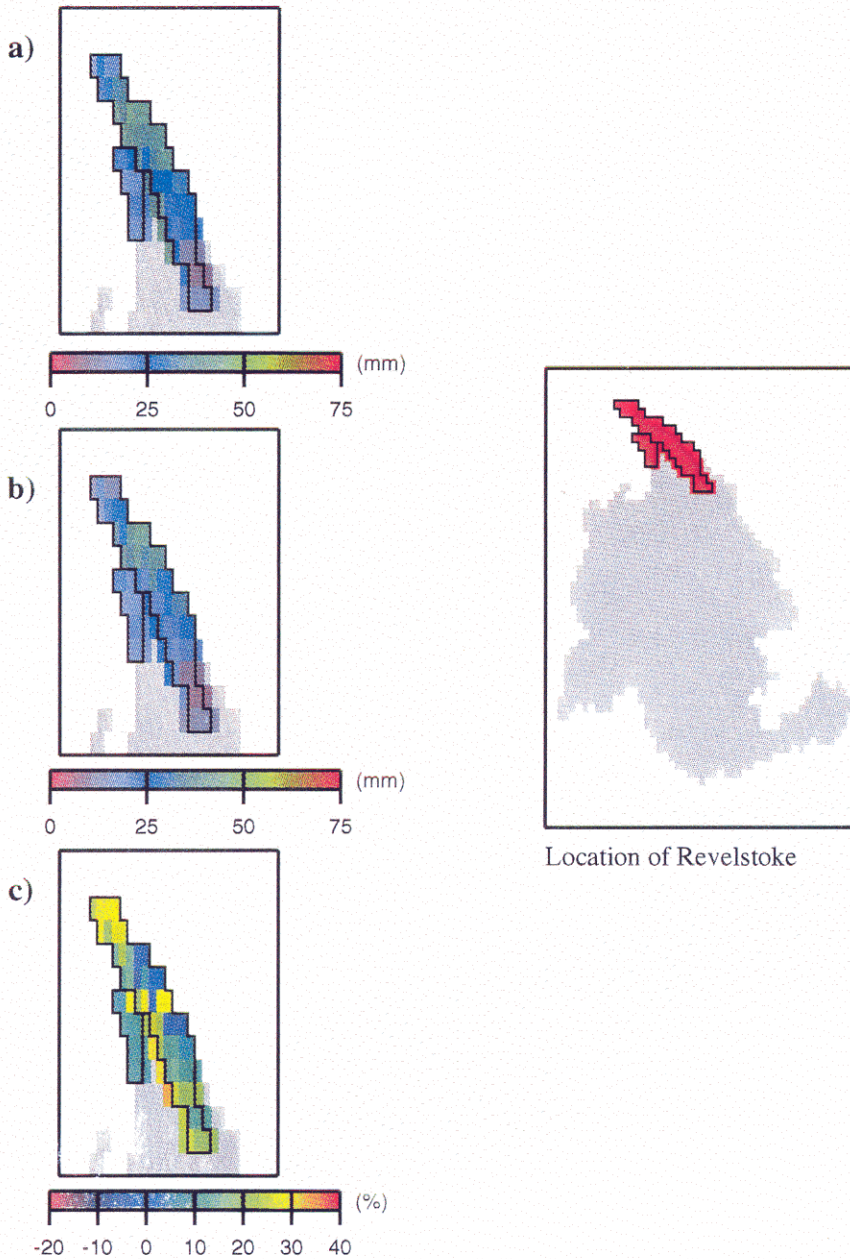


Figure 5.3 Simulated mean monthly a) current, b) historical and c) percent difference in baseflow for the month of October at Revelstoke.

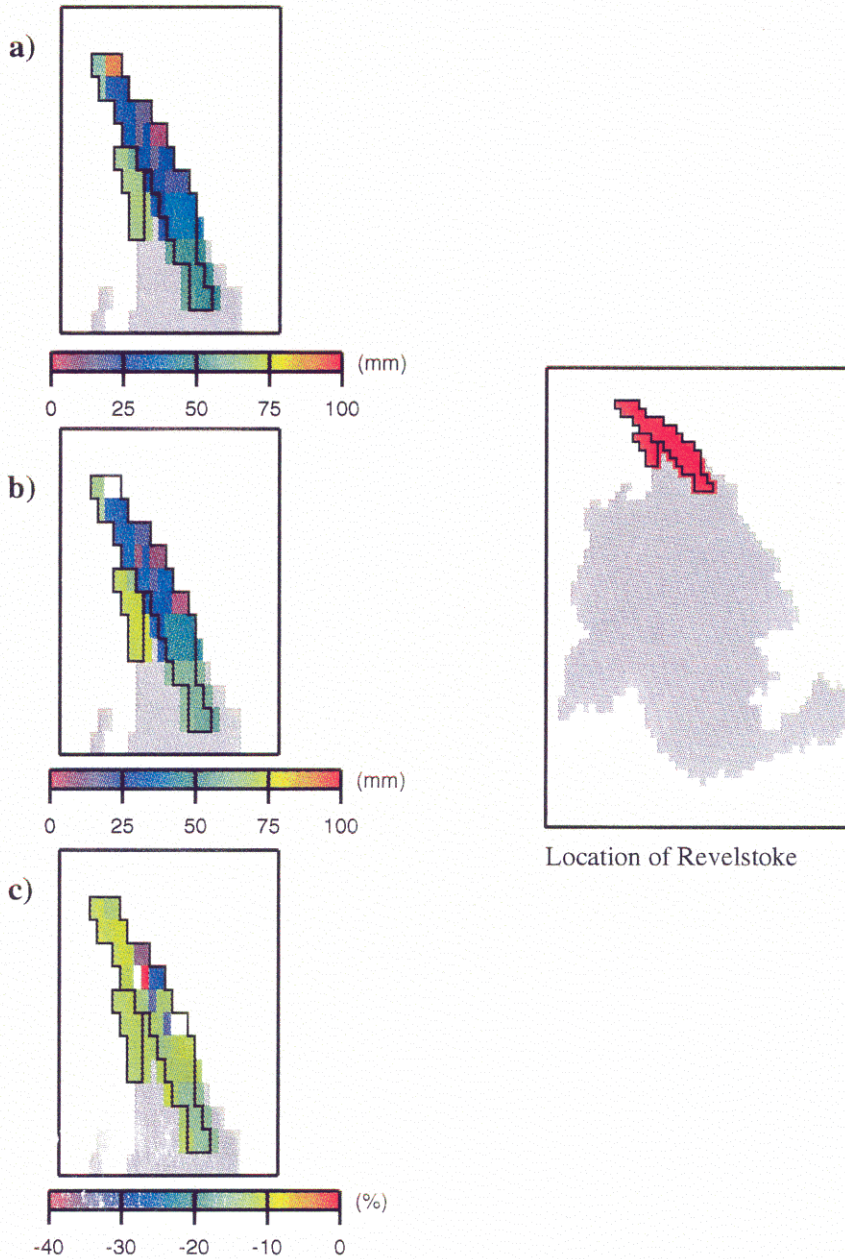


Figure 5.4 Simulated mean monthly a) current, b) historical and c) percent difference in evaporation for the month of May at Revelstoke.

The current and historical hydrographs at Corra Linn show a similar result in the summer as those for Mica and Revelstoke, with high historical scenario summer evaporation influencing the large summer RPD. Differences in the current and historical hydrographs level off quickly in the beginning of fall and remain within 5 percent for the remainder of the year. This sharp reduction in RPD in the fall is attributed to the thick total soil layer, and particularly bottom soil layer, defined by the soil parameters for this region. The subbasin average total soil moisture storage capacity, $W_{c,tot}$ is 1,200 mm and bottom layer soil moisture storage capacity is 800 mm, allowing for the baseflow to quickly recharge in the historical scenario following high summer evaporation and equilibrate with the current scenario baseflow.

The largest overall differences in runoff between the current and historical scenario simulations were for the region drained by Waneta, with a long term annual decrease in simulated runoff of 10 percent. Historically, grasses and forbs (broad-leafed plants, including weeds and wildflowers) covered much of the central part of the subbasin, with late coniferous forest, moderate drought tolerance (CFM-Late), late coniferous forest, drought tolerant (CFT-late) and middle structural stage conifers with moderate to high drought tolerance (CFM-Middle and CFT-Middle) interspersed. In the current scenario, the grasses and forbs are replaced with middle structural stage, drought tolerant conifers. Middle structural stage tolerant and moderately tolerant coniferous species occur in place of the historical late structural stage coniferous forests. Table 5.3 summarizes the differences in vegetation parameters corresponding with the respective changes in

vegetation.

Table 5.3 Current and historical scenario vegetation parameters at Waneta.

	Current	Historical	Current	Historical	Current	Historical
VIC-2L vegetation cover class	CFT- Middle	G/F- Shrub	CFT- Middle	CFT- Late	CFM- Middle	CFM- Late
LAI _{max}	6.0	1.5	6.0	5.0	9.0	7.0
Height (m)	15.0	1.0	15.0	30.0	17.5	35.0
r_s (m/s)	166.6	125.0	166.6	166.6	166.6	166.6
r_{arc} (m/s)	40.0	2.5	40.0	40.0	40.0	40.0
f2 (%)	55	20	55	55	55	55

The shift from grasses and forbs to CFT-Middle results in the largest differences in vegetation parameters within the region, and results in significantly higher annual evaporation in the current scenario. The other dominant shifts in vegetation also contribute to substantially higher current scenario evaporation. Large differences in the monthly hydrographs persist throughout the year as a result of high year round current scenario evaporation and lower baseflow.

The hydrographs at Chief Joseph and Priest Rapids show the same trend in

monthly RPD as shown for Corra Linn, but the magnitude of the changes are somewhat smaller. This overall reduction in RPD is due to the upstream influence from Waneta, which experiences large negative values of mean annual RPD. As a result of the superposition of hydrographs from Corra Linn, Waneta and the remaining upstream area, Chief Joseph and Priest Rapids experience small mean annual differences in simulated runoff of 0.9 and 2.0, respectively, despite relatively large seasonal variation in RPD.

The Oxbow and Ice Harbor regions show substantial shifts in vegetation between the historical and current scenarios, but low monthly and annual RPD. The dominant vegetation change in this region has been conversion of grasses and forbs to agriculture. Because the effects of agricultural irrigation are not included in the model, comparison of simulated current and historical scenario streamflow is somewhat artificial. Additional shifts in vegetation occurred over smaller areas, including conversion of drought tolerant shrubs (ST) and middle structural stage, moderately drought tolerant coniferous forest (CFM-Middle) to middle structural stage, moderately drought tolerant deciduous trees (DFM-Middle) in the eastern portion of Oxbow and conversion of late, drought tolerant coniferous forest (CFT-Late) to middle, moderately drought tolerant coniferous forest (CFM-Middle) near the border between Oxbow and Ice Harbor. Although these changes are extensive in terms of spatial extent, the resulting differences in parameters are relatively small. Furthermore, the hydrographs at Oxbow and Ice Harbor are limited by low mean annual precipitation. Thus, the effect of changes in vegetation on streamflow is masked by the effect of low moisture input for both the current and historical scenarios.

Finally, the hydrographs at The Dalles have a somewhat damped seasonal variation in monthly RPD, with small positive values in the spring and summer and small negative values in the fall and winter. Downstream from Priest Rapids, the incremental effects of changes in vegetation are relatively small, as suggested by the similarity in hydrographs between Priest Rapids and The Dalles. Over the long term annual cycle, The Dalles experienced a RPD of 0.75 percent.

5.2.1.1 Sensitivity analysis of the root distribution parameter

The vegetation parameter f_2 apportions a percentage of the total root zone depth to the bottom model soil layer. Since there are only two soil layers, the percentage of the total root depth contained in the top soil layer, f_1 , is $1-f_2$. A sensitivity analysis of f_2 with respect to varying structural stage was performed in order to assess the importance of representing changes in the vertical extent of roots as a stand transitions into successive structural stages. This analysis was performed in two stages. In the first stage, a single point was analyzed for the period October, 1980 to September, 1995 in order to evaluate the effect of varying f_2 on water partition at the grid cell scale. In the second phase of this analysis, the effect of varying f_2 was analyzed for Corra Linn (see Figure 4.5 for location of Corra Linn) for the test period October, 1986 to September, 1989 in order to assess how the differences in water partition at the grid-cell scale aggregate and ultimately affect simulated hydrographs at the subbasin scale.

According to conversations with Tom Hinckley (Professor in the College of Forest Resources, University of Washington), the vertical extent of roots within a stand is fully developed by the time of stem exclusion, which is associated with the middle structural stage as defined here. Accordingly, f_2 was only varied between the early and middle structural stages for both the point and subbasin analyses. For forested cover types, $f_{2_{late}}$ was assumed to equal $f_{2_{middle}}$. Thus, f_2 variability was expressed as:

$$f_2 \text{ variability} = f_{2_{early}} - f_{2_{middle/late}} \quad (22)$$

where the functionality is with respect to forest cover type. The second term applies to the middle and late structural stages combined. The value for $f_{2_{early}}$ was held constant at 50% for all runs. $f_{2_{middle/late}}$ was varied between 40% and 75% in increments of 2.5%. All other vegetation parameters were held constant. For the point sensitivity study, the soil parameters used are summarized in Table 5.4.

Table 5.4 Soil parameter used values for the point sensitivity analysis of f2.

Parameter name	Symbol	Units	Range
Infiltration Parameter	bi		0.25
Total soil moisture	Wc	mm	1500
Fraction of maximum baseflow	Ds		0.05
Maximum baseflow	Dm	mm/day	10
Fraction of maximum baseflow at which baseflow computation becomes non-linear	Ws		0.8
Ratio of soil moisture in bottom layer to top layer	$W_{1/2}$		1.5
Saturated hydraulic conductivity	Ks	mm/day	250

Figure 5.5 shows results from the point sensitivity analysis for the month of August. Long-term mean monthly VIC-2L outputs, including total evaporation, soil moisture in the upper and lower soil layers (W_1 and W_2 , respectively), baseflow and runoff, are shown as a function of variable $f2_{middle/late}$. Baseflow and runoff were summed to produce total runoff, which is analogous to streamflow for a single grid cell. The secondary axis shows the response of the relative percent difference (RPD) for each variable between the current and historical scenario predictions to changes in $f2_{middle/late}$.

where RPD is expressed in terms of the current scenario values. All variables (other than evaporation) show a step function response to changes in $f2_{\text{middle/late}}$, with a threshold value of $f2_{\text{middle/late}} > 50.0\%$ causing a sharp response in RPD. For instance, relative percent difference for W1 remains approximately zero for values of $f2_{\text{middle/late}}$ below the threshold and jumps to -7% after $f2_{\text{middle/late}}$ crosses the threshold. Similarly, a sharp decrease in RPD occurs for runoff with values of $f2_{\text{middle/late}}$ in excess of the threshold. The integrated effect of varying $f2$ as a function of structural stage at the grid-cell scale is shown in the RPD response of total runoff, which jumps from 6% to 11% with variation in $f2_{\text{middle/late}}$ above 50% .

Figure 5.6 shows the same information as above for April. In this figure, the step function response in RPD is apparent for evaporation, with a -10% RPD below the threshold and -15% RPD above the threshold. The other variables, including total runoff, show relatively small response to variations in $f2_{\text{middle/late}}$. This lower degree of response in RPD for total runoff in the early spring as compared with mid-summer illustrates that the sensitivity of the model to the parameterization of the rooting zone is highest when net radiation and evaporation are highest.

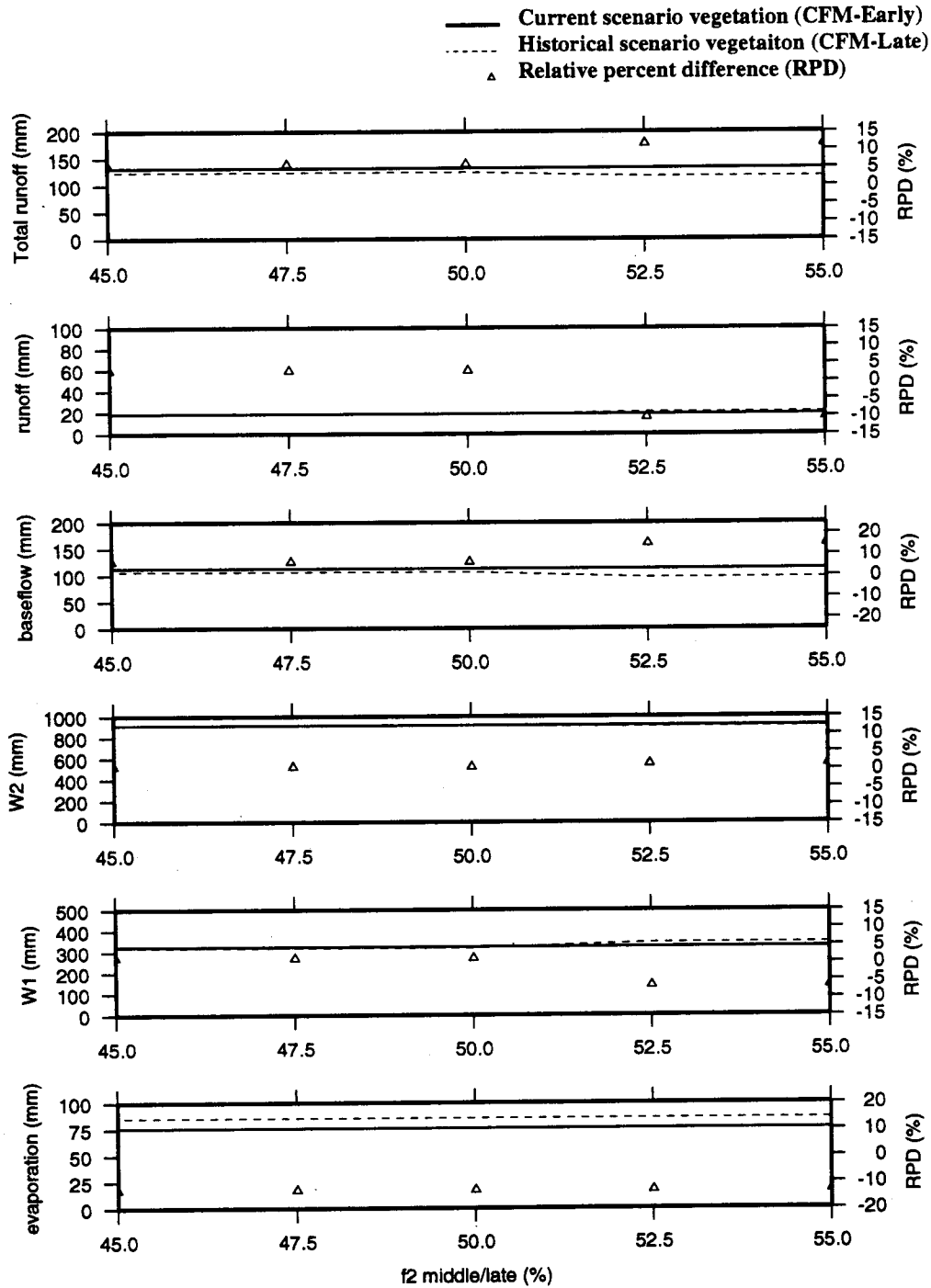


Figure 5.5 VIC-2L results from point sensitivity analysis for the month of August.

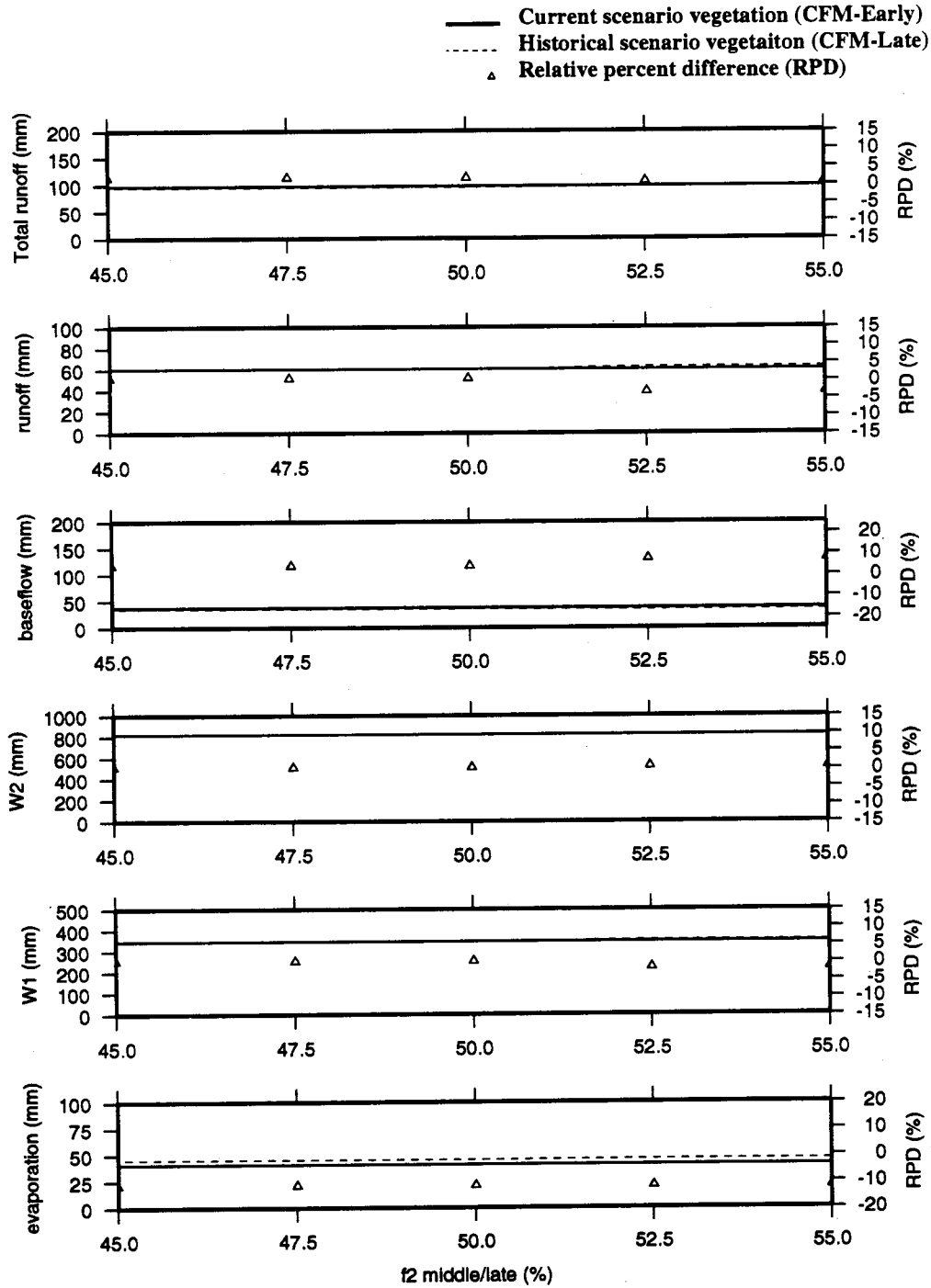


Figure 5.6 VIC-2L results from point sensitivity analysis for the month of May.

In the second phase of this study, f_{2_early} was held at 50% and $f_{2_middle/late}$ was varied as described above. All other parameters, including the soil parameters, remained unchanged. Table 5.4 provides the range of soil parameters used for Corra Linn.

Table 5.5 Range of calibrated soil parameters for Corra Linn.

Parameter name	Symbol	Units	Range
Infiltration Parameter	bi		0.25
Total soil moisture	Wc	mm	1200 - 1500
Fraction of maximum baseflow	Ds		0.035 - 0.0475
Maximum baseflow	Dm	mm/day	10 - 11
Fraction of maximum baseflow at which baseflow computation becomes non-linear	Ws		0.7 - 0.95
Ratio of soil moisture in bottom layer to top layer	$W_{1/2}$		1.5 - 2
Saturated hydraulic conductivity	Ks	mm/day	250 - 350

Figure 5.7 shows comparisons of current and historical scenario simulated streamflow corresponding with six incremental variations in $f2_{\text{middle/late}}$. The dashed line represents the relative percent difference between the current and historical streamflow. As was found in the first part of this analysis, the response of RPD to variations in $f2_{\text{middle/late}}$ is a step function. The seasonal trend in monthly RPD is greatly exaggerated for values of $f2_{\text{middle/late}} > 50\%$, as well as the mean annual RPD.

This step function behavior appears to be an artifact of the current version of the model (Liang, 1994), in which transpiration from both model soil layers is expressed as:

$$E_t[n] = f1[n] \cdot E_1^t[n] + f2[n] \cdot E_2^t[n] \quad (23)$$

where, $E_1^t[n]$ and $E_2^t[n]$ are the transpiration rates from the top and bottom layers, respectively, for a given vegetation cover class, n , and the calculation of transpiration from a single soil layer was based on Blondin (1991) and Ducoudre et al. (1993):

$$E_t = \left[1 - \left(\frac{W_i[n]}{W_{im}[n]} \right)^{\frac{2}{3}} \right] \cdot Ep[n] \cdot \frac{r_w[n]}{r_w[n] + r_0[n] + r_c[n]} \quad (24)$$

where, $W_i[n]$ is the amount of water intercepted by the canopy of vegetation class, n , (in mm), $W_{im}[n]$ is the maximum water interception by the canopy of vegetation class, n , $Ep[n]$ is the potential evaporation rate from a thin free water surface (Shuttleworth, 1993), $r_w[n]$ is the aerodynamic resistance to the transfer of water from the canopy to the atmosphere, $r_0[n]$ is the architectural resistance and $r_c[n]$ is the canopy resistance. The canopy resistance integrates the minimum stomatal resistance over the canopy for vegetation class, n , and is calculated as:

$$r_c = \frac{r_{\min}[n] \cdot g_{sm}[n]}{LAI[n,m]} \quad (25)$$

where, $r_{\min}[n]$ is the minimum stomatal resistance, $g_{sm}[n]$ is a soil moisture stress factor dependent on available moisture in the root zone for a cover class, n , and $LAI[n,m]$ is the monthly LAI for the cover class, n . The reader is referred to Liang (1994) for a more complete description of these formulations.

There are three general solutions to Equation 23, corresponding with three physical cases. The form of the solution for the first two cases is dependent upon the value of f_2 , the actual moisture stored in both soil layers, W_1 and W_2 , and the maximum soil moisture storage capacity for both soil layers, determined by $W_{c,tot}$ and $W_{2/1}$. In the first case (i), the following conditions must be met: $W_2 \geq W_2^{cr}$ and $f_2 \geq 50\%$, where W_2^{cr} is analogous with the field capacity of the bottom soil layer and is taken as 58 percent of the maximum soil moisture in the bottom layer, W_2 . Under this scenario, transpiration occurs from the bottom soil layer with $g_{sm}[n] = 1.0$. Transpiration from the upper layer, $E_1^i[n]$, is set to 0.0, regardless of moisture availability and/or depth of roots in the upper layer. The second case requires: $W_1 \geq W_1^{cr}$ and $f_1 \geq 50\%$, and is only valid if the criteria for case (i) are not met. Under this scenario, transpiration is supplied by the top soil layer only (i.e., $E_2^i[n] = 0.0$) and soil moisture stress is negligible. The third case (iii) applies in the event that the criteria for cases (i) and (ii) are not met. Under this final scenario, transpiration from each soil layer occurs independently of the other layer

following Equations 23 and 24, with soil moisture stress calculated as a function of the actual soil moisture content in layer $j=1,2$, $W_j[n]$, the critical soil moisture, W_j^{cr} and permanent wilting point, W_j^w for layer $j=1,2$:

$$g_{sm}[n] = 1.0 \quad \text{for } W_j[n] \geq W_j^{cr} \quad (26)$$

$$g_{sm}[n] = \frac{W_j[n] - W_j^w}{W_j^{cr} - W_j^w} \quad \text{for } W_j^w \leq W_j[n] < W_j^{cr} \quad (27)$$

$$g_{sm}[n] = 0.0 \quad \text{for } W_j[n] < W_j^w \quad (28)$$

The value of $f1/f2 = 50\%$, which partially determines whether case (i), case (ii) or case (iii) will be used, was adopted arbitrarily.

A more realistic approach to calculating transpiration would be to always assume case (iii). With this approach, transpiration is supplied by both soil layers provided that $W_j[n] \geq W_j^{wr}$ for $j=1,2$ and that the vegetation roots penetrate both soil zones. According to Equation 23, the distribution of roots within the two model soil compartments (i.e., the values $f1$ and $f2$) governs the relative contribution of each soil layer to transpiration. Thus, if a vegetation type has shallow roots, such as grasses, forbs, shrubs and agriculture, only the top model soil layer contributes significantly to transpiration. On the other hand,

forest vegetation, which generally has deeper roots, would extract water from either or both soil layers, depending on the availability of water in each layer. Representing subgrid variability in the soil moisture stress factor, g_{sm} , for the upper soil zone would further improve the calculation (see Liang, 1994 for details). It can be expected that an improved method for computing transpiration would reduce predicted seasonal and annual changes in streamflow, as was seen in the sensitivity analysis for Corra Linn with values of $f2_{middle/late}$ below the critical value.

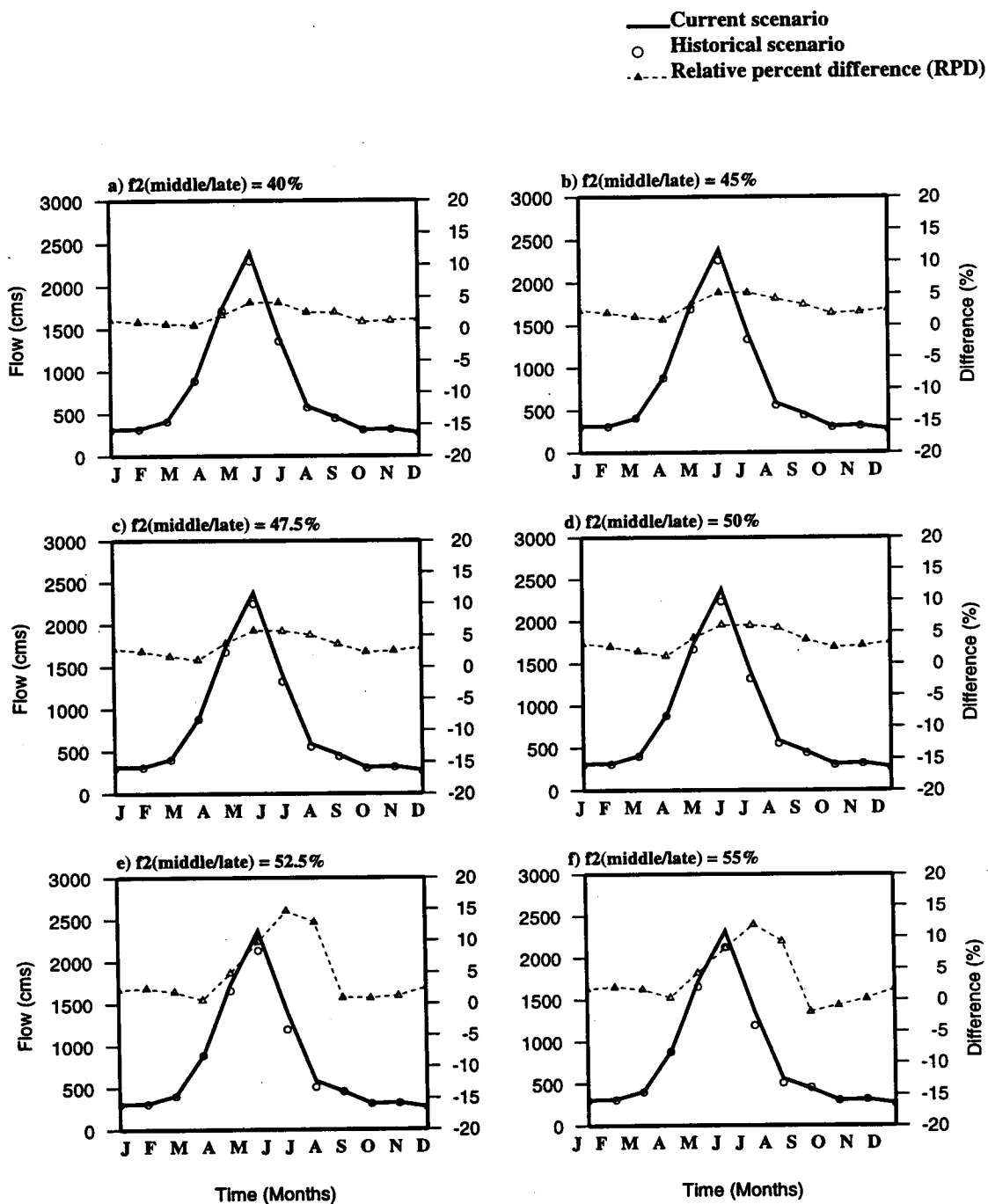


Figure 5.7 Sensitivity analysis of vegetation parameter f_2 performed for Corra Linn for the test period October, 1986 to September, 1989.

6. Conclusions

The VIC-2L model was applied to the portion of the Columbia River basin upstream of The Dalles at quarter-degree resolution. Model performance was based on comparisons of simulated and naturalized streamflow at nine locations within the basin for the calibration and test periods, October, 1983 - September, 1986 and October, 1986 - September, 1989, respectively. Model performance was generally comparable to that obtained in a prior coarser resolution application of the model (by Nijssen et al., 1997), with good reproduction of natural flows at most main stem Columbia River locations. Poorest model performance occurred at Oxbow and Ice Harbor on the Snake River, which are dominated by groundwater effects and are the driest regions within the basin. The modeled and naturalized hydrographs at Waneta were in best agreement in terms of timing and magnitude of long-term mean peak flows. The natural hydrograph at Waneta is typical of the CRB, with a peak flow in spring roughly five times greater than the mean annual baseflow. Problems with timing of peak flow at Corra Linn, Chief Joseph, Priest Rapids and, ultimately, at The Dalles were attributed to poor timing of spring snowmelt at Corra Linn. Generally, model performance was comparable between the calibration and test periods.

Once the model was calibrated and tested, it was implemented for the entire period of the meteorological data record, October, 1980 to September, 1995 for the current and historical vegetation scenarios. The vegetation scenarios were represented by the

assignment of parameters, which was based on spatial vegetation class maps for the current and historical scenarios at quarter degree resolution. These vegetation class maps were derived by processing existing current and historical scenario maps at 1-km spatial resolution. A look-up table was used to relate parameter values with vegetation classes for the current and historical scenarios. The resulting current and historical scenario vegetation parameters formed the basis for analyzing differences in streamflow.

Differences in the current and historical hydrographs were expressed in terms of relative percent difference (RPD) with respect to the current scenario hydrograph. The results may be summarized as follows:

- For the Columbia River at The Dalles, predicted changes in mean annual streamflow were very small (<1 percent).
- Positive mean annual RPD was highest in the upper portion of the basin, including Mica, Revelstoke and Corra Linn, with an average mean annual RPD of 6 percent and large seasonal variation throughout the year. Highest seasonal RPD at these locations occurred in the summer, which was attributed to increased historical summer evaporation caused by conversion of late structural stage coniferous forest to early structural stage coniferous forest between the historical and current vegetation scenarios.

- A negative mean annual RPD of 10 percent was predicted at Waneta, and is related to a conversion of grasses and forbs to coniferous forest in the central part of the subbasin. This shift in vegetation resulted in significantly higher current scenario evaporation and lower baseflow year-round.
- While Oxbow and Ice Harbor experienced shifts in vegetation over most of the region, the resulting changes in parameters were insignificant. As a result, and in combination with low mean annual precipitation, monthly RPD remained roughly within 5 percent and mean annual RPD remained within 3 percent for both of these regions.
- The predicted changes in streamflow were highly sensitive to the parameterization of the vegetation rooting zone in the two model soil layers. A more physically realistic approach to calculating transpiration may result in lower seasonal variation in RPD as well as lower mean annual RPD in regions which are not moisture limited.

7. References

A.G. Crook Company, Technical Appendix for development of modified streamflows, 1928-1989, Columbia River and Coastal Basins, prepared for Bonneville Power Administration, June, 1993.

Agee, J.K., Fire and weather disturbances in terrestrial ecosystems of the eastern Cascades, USDA Forest Service Gen. Tech. Rep. PNW-GTR-320. Pacific Northwest Research Station, Portland, Oregon, 1993.

Anderson, E. A., National Weather Service river forecast system - snow accumulation and ablation model, NOAA Technical Memorandum NWS HYDRO-17, U.S. Department of Commerce, 1973.

Avisar, R. and Pielke, R.A., A parameterization of heterogeneous land surfaces for atmospheric numerical models and its impact on regional meteorology, *Monthly Weather Review*, 117, pp. 2113-2135, Oct. 1989.

B.P.A., 1990 Level Modified Streamflow 1928-1989, diversion and return flow patterns, summation of depletion adjustments, evaporation adjustments, Columbia river and coastal basins, Bonneville Power Administration, April, 1993.

B.L.M., CRBSUM Current Vegetation Cover Types (ASSESS), created by Intermountain Fire Sciences Laboratory, April 30, 1996.

Bras, R.L., *Hydrology, an introduction to hydrologic science*, Addison-Westley, Reading, etc. 1990.

Burns, Russell M. and Honkala, Barbara H., *Silvics of North America, agriculture handbook 654, Vol. 1*, Forest Service, United States Department of Agriculture, Washington D.C., December, 1990.

Calder, I.R., *Hydrologic effects of land-use change*, Chapter 13 in *Handbook of Hydrology*, D. R. Maidment, ed., McGraw-Hill, Inc., U.S.A., 1993.

Chase, Thomas N. and Roger A. Pielke, Kittel, T.G.F., Nemani, R and Running, S.W., *Sensitivity of a general circulation model to global changes in leaf area index*, *J. of Geophys. Res.*, vol 101, no. D3, pp. 7393-7408, Mar. 20, 1996.

Copeland, Jeffrey H. and Pielke, R.A., Kittel, T.G.F., *Potential climatic impacts of vegetation change: A regional modeling study*, *J. of Geophys. Res.*, vol 101, No D3, pp. 7409-7418, Mar. 20, 1996.

Daly, C., T.P. Neilson, and D.L. Phillips, *A statistical-topographic model for mapping climatological precipitation over mountainous terrain*, *J. Appl. Met.*, 33, pp. 140-158, 1994.

DeFries, R.S., and J.R.G. Townshend, *NDVI-derived land cover classifications at a global scale*, *Int. J. Rem. Sens.*, 15, 17, pp.3567-3586, 1994.

Dickinson, R.E., A. Henderson-Sellers, P.J. Kennedy, and M.F. Wilson, *Biosphere-atmosphere transfer scheme (BATS) for the NCAR community climate model*, NCAR Tech. Note, TN-275+STR, 1986.

Ducoudre, N. I., K. Laval, and A. Perrier, *SECHIBA, a new set of parameterizations of the hydrologic exchanges at the land-atmosphere interface within the LMD atmospheric general circulation model*, *J. Clim.*, 6, pp.248-273, 1993.

Duncan, S. H., Peak stream discharge during thirty years of sustained yield timber management in tow fifth order watersheds in Washington State, Northwest Science, Vol. 60, No. 4, 1986.

Earthinfo Inc., Climatedata , Summary of the day, NOAA, NCDC, Volume 3, Earthinfo Inc., 1991.

Eltahir, E.A.B. and Bras, R.L., On the response of the tropical atmosphere to large-scale deforestation, Q.J.R. Meteorol. Soc., 119, pp. 779-793, 1993.

Francini, M. and M. Pacciani, Comparative analysis of several conceptual rainfall-runoff models, J. Hydrol., 122, 161-219, 1991.

Fuls, E.R., Ecosystem modification created by patch-overgrazing in semi-arid grassland, J. of Arid Environments, 23(1), pp 59-69, 1992.

Ferguson, B.K., Changing rainfall-runoff relationships in the urbanizing Peachtree Creek Watershed, Atlanta, Georgia, Water Resources Bulletin, 1990 vol. 26, no. 2, pp. 313-322, 1990.

Furniss, M.J., T.D. Roelofs and C.S. Yee, Road construction and maintenance. American Fisheries Society Publication 19:297-324, 1991.

Harr, R. Dennis, Effects of clearcutting on rain-on-snow runoff in Western Oregon: A new look at old studies, vol. 22, no. 7, pp. 1095-1100, July, 1986.

Haynes, R.W. and A.L. Horne, Economic assessment of the Interior Columbia Basin. In Quigley, T.M and S.J. Arbelbide, tech. Eds., An assessment of ecosystem components in the Interior Columbia Basin including portions of the Klamath and Great Basins. USDA Forest Service, Pacific Northwest Research Station, Portland, OR, 1996.

Henderson-Sellers A., Continental vegetation as a dynamic component of a global climate model: A preliminary assessment, *Clim. Changes*, 23, pp. 337-377, 1993.

Henderson-Sellers, A., Yang, Z.L. and Dickinson, R.E., The project for intercomparison of land-surface parameterization schemes, *Bull. of the Am. Meteorol. Soc.*, col. 74, no 7, pp.1335-1349, July, 1993.

Hessburg, Paul and Smith, Brad, Midscale landscape dynamics of the interior Columbia River basin, *Landscape Ecology Stars Report*, Portland OR, U.S. Department of Agriculture, forest Service, Pacific Northwest Research Station, 1996.

Heyerdahl, Emily K., D. Berry and J.K. Agee, Fire history database of the Western United States, Interagency agreement DW12934530, U.S. EPA, USDA Forest Service and University of Washington, September, 1995.

Hicks, B.J., P.A. Hall, P.A. Bisson and J.R. Sedell, Responses of salmonids to habitat changes. In *Influences of forest and rangeland management on salmonid fishes and their habitats*. American Fisheries Society Special Publication 19:483-518, 1991.

Hinckley, T.M., J.P. Lassouie, and S.W. Running, Temporal and spatial variations in the water status of forest trees, *Forest Science* 24(3):1-72, 1978.

Jones, J.A. and G.E. Grant, Peak flow responses to clear-cutting and roads in small and large basins, western Cascades, Oregon, *Water Resources Research*, Vol. 32, No. 4, pp. 959-974, April, 1996.

Kelliher, F.M., R. Leuning, M.R. Raupach, and E.D. Schulze, Maximum conductances for evaporation from global vegetation types, *Agricultural and Forest Meteorology*, 73:1-16, 1995.

Keppeler, Elizabeth T. and Ziemer, Robert R., Logging effects on streamflow: Water yield and summer low flows at Casper Creek in Northwestern California, *Wat. Resources Res.*, vol. 26, No. 7, pp. 1669-1679, July, 1990.

Korner, C.H., J.A. Schell, and H. Bauer, Maximum leaf diffusive conductance in vascular plants, *Photosynthetica* 13:45-82, 1979.

King, John G. and Tennyson, Larry C., Alteration of streamflow characteristics following road construction in North Central Idaho, *Wat. Resources Res.*, vol. 20, no. 8, pp. 1159-1163, Aug. 1984.

Kuhl, S.S., and J. r. Miller, Seasonal river runoff calculated from a global atmospheric model, *Wat. Resour. Res.*, 28, pp. 2029-2039, 1992.

Larson, David N. and P. Gobroski, Washington timber harvest, 1993, Washington State Department of Natural Resources, 1995.

Lassoie, J.P., T.M. Hinckley and C.C. Grier, Coniferous forests of the Pacific Northwest in physiological ecology of North American plant communities eds. B.F. Chabot and H.A. Mooney, Chapman and Hall, Mew York, 351 pp.

Lean, J. and P.R. Rowntree, A GCM simulation of the impact of Amazonian deforestation on climate using an improved canopy representation, *Q.J.R. Meteorol. Soc.*, 119, pp.509-530, 1993.

Lettenmaier, D.P., and E. F. Wood, Implementation of the VIC-2L Land Surface Scheme to Model the Hydrology of Large Continental Rivers, report to Electric Power Research Institute, Dec., 1994.

Lewis, H.T., Why indians burned: Specific versus general reasons, in Lotan, J.E., Kilgore, W.C., Fisher, W.S., Mutch, R.W., Symposium and workshop on wilderness fire. U.S. Department of Agriculture Gen. Tech., Rep. INT-182, 1985.

- Lohmann, D. , E. Raschke, B. Nijssen, D. P. Lettenmaier, Regional scale hydrology: Application of the VIC-2L model to the Weser River, Germany, paper submitted to J. Hyd. Sci., 1996.
- Loveland, T. R., J.W. Merchant, D.O. Ohlen, and J.F. Brown, Development of a land-cover characteristics database for the conterminous U.S., Photogramm. Eng. Remote Sense., 57, 1453-1463, 1990.
- Li, Bin and Avissar, R., The impact of spatial variability of land-surface characteristics on land-surface heat fluxes, J. of Clim., vol 7, pp. 527-537, April 1994.
- Liang, Xue and D.P. Lettenmaier, E. F. Wood, and S. J. Burges, A simple hydrologically based model of land surface water and energy fluxes for general circulation models, J. Geophys. Res., 99, D7, pp. 14,415-14,428, 1994.
- Liston, G. E., Y. C. Sud, E. F. Wood, Evaluating GCM land surface hydrology parameterizations by computing river discharges using a runoff routing model: application to the Mississippi basin, J. Appl. Met., 33, pp. 394-405, 1994.
- Losensky, B. John, Historical vegetation types of the interior Columbia River basin, Forest Service, U.S. Department of Agriculture, Ecological Services, December, 1994.
- Lyons, T.J., Schwerdtfeger, P., Hacker, J.M., Foster, I.J., Smith, R.C.G., and Xinmel, Huang, Land atmosphere interaction in a semiarid region: the bunny fence experiment, Bull. of the Am. Meteorol. Soc., vol 74, no 7, 1327-1334, July, 1993.
- Manzi, A. O. and S. Planton, Implementation of the ISBA parameterization scheme for land surface processes in a GCM – an annual cycle experiment, J. Hydr., 155, pp. 353-387, 1994.

Megahan, Walter F., Effects of forest roads on watershed function in mountainous areas, Proceedings of the Symposium on Environmental Geotechnics and Problematic Soils and Rocks, Bangkok, Dec. 1985.

Megahan, Walter F., Hydrologic effects of clearcutting and wildfire on steep granitic slopes in Idaho, Wat. Resources Res., vol 19, no.3, pp. 811-819, June 1983.

Miles, T.G and M.G. Karl, Introduced forage grasses in the Interior Columbia Basin: Science assessment. Unpublished report on file with the Interior Columbia Basin Ecosystem Management Project, Walla Walla, Wa., 1995.

Naeth, M.A., D.J. Pluth, D.S. Chanasyk, A.W. Bailey and A.W. Fedkenheuer, Soil compacting impacts of grazing in mixed prairie and fescue grassland ecosystems of Alberta. Can. J. Soil Sci. 70:157-167, 1990.

NOAA- Airborne and Satellite Snow Data, National Operational Hydrologic Remote Sensing Center, Office of Hydrology, National Weather Service, NOAA, Minneapolis, Mn., 1990-1995.

Pellant, M. and Hall, C., Distribution of two exotic grasses on intermountain rangelands: Status in 1992. In Monsen, Kitchen eds. Proceedings-ecology and management of annual rangelands. USDA Forest Service, Intermountain Research Station, Ogden, Ut., Gen Tech. Rep. INT-GTR-3134, 1994.

Peterson, K., River of Life Channel of Death: Fish and Dams on the Lower Snake., Lewiston, Id., Confluence Press, Inc., 1995

Quigley, T.M and S.J. Arbelbide, tech. Eds., An assessment of ecosystem components in the Interior Columbia Basin including portions of the Klamath and Great Basins. USDA Forest Service, Pacific Northwest Research Station, Portland, OR, 1996.

Schulte, P.J. and T.M. Hinckley, Abscisic acid relations and the response of *Populus trichocarpa* stomata to leaf water potential, *Tree Physiology*, 3:103-113., 1987.

Shiflet, T.N., (ed.). Society of Range Management, Denver, Colorado, 1994.

Sellers, P.J., Y. Mintz, Y. C. Sud, and A. Dalcher, A simple biosphere model (SiB) for use within general circulation models, *J. Atmos. Sci.*, 43, pp. 505-531, 1986.

Sellers, P.J., S.O. Los, C.J. Tucker, C.O. Justice, D.A. Dazlich, G.J. Collatz and D.A. Randall, A revised land surface parameterization (SiB2) for atmospheric GCMs. Part II: The generation of global fields of terrestrial biophysical parameters from satellite data, *J. of Clim.*, 9, pp 706-737, 1996.

Sias, J. C and Lettenmaier, D. P., Potential Effects of Climatic Warming on the Water Resources of the Columbia River Basin, Water Resources Series, Technical Report No. 142, October, 1994.

Rothacher, Jack, Increases in water yield following clear-cut logging in the Pacific Northwest, *Wat. Resources Res.*, vol 6, no 2, pp. 653-658, April, 1970.

Shuttleworth, W. J., Evaporation, chapter 4 in *Handbook of Hydrology*, D. R. Maidment, ed., McGraw-Hill, Inc., New York, etc., 1993.

Spence, C., A. Dalton, and Kite, G., GIS supports hydrological modeling, *GIS World*, 8, pp. 62-65, 1995.

Stamm, J.F. and E. F. Wood, and D. P. Lettenmaier, Sensitivity of a GCM simulation of global climate to the representation of land surface hydrology, *J. Clim.* 7, pp. 1218-1239, 1994.

Stegman, Steven V., Snowpack changes resulting from timber harvest: Interception, redistribution and evaporation, *Wat. Resources Bull.*, vol. 32, no 6, pp. 1353-1360, Dec. 1996.

Sud, Y. C., P. J. Sellers, Y. Montz, M.D. Chou, G.K. Walker and W.E. Smith, Influence of the biosphere on the global circulation and hydrologic cycle - a GCM simulation experiment, *Agric. and Forest Met.*, 52, pp. 133-180, 1990.

Sud, Y. C., and Y. Mintz, Influence of land surface roughness on atmospheric circulation and precipitation: A sensitivity study with a general circulation model, *J of Appl. Met.*, 27, pp. 1036-1054, 1988.

Sud, Y.C., Yang, R. and Walker, G.K., Impact of in situ deforestation in Amazonia on the regional climate: General circulation model simulation study, *J. of Geophys. Res.*, vol 101, No D3, pp. 7095-7109, Mar. 20, 1996.

U.S. Department of Energy, Bonneville Power Administration, U.S. Department of the Army, Corps of Engineers, North Pacific Division, U.S. Department of the Interior, Bureau of Reclamation, Pacific Northwest Region, *The Columbia River System: The Inside Story*, 1991.

Wallis, J.R., D.P. Lettenmaier, and E.F. Wood, A daily hydroclimatological data set for the continental United States, *Water Resour. Res.*, 27, 1633-1657, 1991.

Waring, R.H. and J.F. Franklin, The evergreen coniferous forest of the Pacific Northwest., *Science* 204:1380-1386, 1979.

Warren, D.D., Production, Prices, Employment and Trade in Northwest forest industries, third quarter, 1996, USDA Forest Service, Pacific Northwest Research Station, Resource Bulletin PNW-RB-223, February, 1997.

Wigmosta, M., L. Vail, and D. P. Lettenmaier, A distributed hydrology-vegetation model for complex terrain, *Wat. Resour.*, 30, pp. 1665-1679, 1994.

Wood, E. F. Global scale hydrology: Advances in land surface modeling, *Rev. of Geoph.*, Supplement, pp. 193-201, 1991.

Woolfenden, W.B., Historical Ecology and the human dimension in ecosystem management, Manuscript, U.S. Forest Service, Inyo National Forest, 1993.

Xue, Yongkan and Fennessy, M.J. and Sellers, P.J., Impact of vegetation properties on U.S. summer weather prediction, *J. of Geophys. Res.*, vol 101, No. D3, pp. 7419-7430, Mar 20, 1996.

Zhao, R. J., Y.L. Zhang, L. R. Fang, X. R. Liu, and Q. S. Zhang, The Xinanjiang model, in hydrological forecasting, Proceedings Oxford symposium, IAHS Publication 129, pp. 351-356, 1980.